

GraphToxin: Reconstructing Full Unlearned Graphs from Graph Unlearning

Ying Song and Balaji Palanisamy
*University of Pittsburgh
 Pittsburgh, PA, USA*

Abstract

Graph unlearning has emerged as a promising solution to comply with “the right to be forgotten” regulations by enabling the removal of sensitive information upon request. However, this solution is not foolproof. The involvement of multiple parties creates new attack surfaces, and residual traces of deleted data can still remain in the unlearned graph neural networks (GNNs). These vulnerabilities can be exploited by attackers to recover the supposedly erased samples, thereby undermining the intended functionality of graph unlearning.

In this work, we propose GraphToxin, the first full graph reconstruction attack against graph unlearning. Specifically, we introduce a novel curvature matching module to provide fine-grained guidance for unlearned graph recovery. We demonstrate that GraphToxin can successfully subvert the regulatory guarantees expected from graph unlearning—it can recover not only a deleted individual’s information and personal links but also sensitive content from their connections, thereby posing substantially more detrimental threats. Furthermore, we extend GraphToxin to multiple-node removal under both white-box and black-box settings, showcasing its practical feasibility and potential to cause considerable harm.

We highlight the necessity of worst-case analysis and propose a systematic evaluation framework to assess attack performance under both random and worst-case node removal scenarios. Our extensive experiments demonstrate the effectiveness and flexibility of GraphToxin. Notably, existing defense mechanisms are largely ineffective against this attack or even amplify its performance in some cases. Given the severe privacy risks posed by GraphToxin, our work underscores the urgent need for more effective and robust defenses.

1 Introduction

Graph neural networks (GNNs) have demonstrated remarkable success across diverse domains, including social network analysis, drug discovery, and financial risk management [24]. Their strength lies in capturing complex structural dependen-

cies through iterative message passing. However, this mechanism inherently amplifies the risk of sensitive information leakage, raising significant user privacy concerns. Concurrently, data protection regulations such as the General Data Protection Regulation (GDPR) [14] enforce the “right to be forgotten”, requiring GNNs’ to remove personal data upon request. These privacy and legal imperatives have spurred the rapid emergence of graph unlearning (GU) [3].

Graph unlearning aims to remove the influence of specific nodes, edges, or subgraphs from a trained GNN while preserving model performance on the remaining graph. Specifically, upon receiving an unlearning request, the model owner typically employs parameter adjustments or gradient-based optimization to mitigate these effects instead of full retraining, which is prohibitively expensive and time-consuming, and subsequently releases the unlearned version. Despite its success, GU inevitably leaves residual traces of the “forgotten” targets. Although such remnants are often small enough to avoid noticeable performance degradation, they can still be exploited by adversaries through membership inference [46] or graph reconstruction attacks, thereby undermining privacy guarantees. Moreover, the involvement of multiple parties further expands the attack surface. For instance, the service providers or platforms can retain copies of the previous models prior to unlearning for legitimate reasons such as backup and debugging, while users can download such models locally on their devices. These decentralized behaviors fundamentally undermine the assurance of GU. In this work, we focus on the most challenging scenario—node unlearning [30] for node-level tasks—and present the first full graph reconstruction attack against graph unlearning (GU-FGRA).

Research Gap—Graph Unlearning To the best of our knowledge, only one prior work [46] has investigated the privacy risks of GU. However, their study is limited to single-edge removal and aims to infer the link membership of a given node pair, rather than reconstructing the full unlearned graph topology. Consequently, their approach solely reveals minimal information and fails to recover confidential or sensitive content encoded in node features. Additionally, they assume

that the adversary has access to partial unlearned/remaining graphs and a shadow graph with a distribution similar to that of the original graph, which are unrealistic in practice due to strict security and privacy policies. Even if partial data were leaked, finding a faithful replica of the original dataset is infeasible and using publicly available data from a different distribution severely degrades the quality of reconstructed graphs due to distributional shifts.

Graph Reconstruction Attack (GRA) With respect to GRA, existing studies primarily focus on inferring link memberships [13, 39]. Only a few attempt to recover sensitive attributes [8, 27] or the full graph topology [26, 52]. This inconsistent terminology can be misleading, as *a true full GRA should reveal all graph components*. Moreover, current research typically rely on access to node embeddings or shadow models, and often assume that sensitive node features or portions of the topology are available for recovery. They also lack comprehensive evaluation, hindering their practical applicability in scenarios such as red-teaming and model auditing.

Machine Unlearning (MU) Existing reconstruction attacks against MU cannot be trivially adapted to GU-FGRA, as the complex topological structures and rich node features in graphs produce entangled patterns during GNN message passing. To date, a few works have explored reconstruction in MU. These efforts are either limited to linear models for exact unlearning [1] or recover only partial removed samples under white-box settings, with poor scalability to multiple-node removal [15]. Under the i.i.d. assumption commonly adopted for tabular data, multiple sample removals can be treated as a sequence of independent single removals. In contrast, graph unlearning is fundamentally different: due to the “ripple effects” propagated through GNNs, even a single node removal can affect its neighbors and higher-order structures, preventing a straightforward extension to GU.

Research Questions The above research gap motivates us to identify three key research questions in GU:

1. Is it possible to recover full unlearned graphs under realistic white-box settings and how this attack can be extended to multiple-node removal?
2. Can this attack be generalized to black-box settings and reconstruct full unlearned graphs using only minimal prior knowledge for multiple-node removal?
3. How can we comprehensively evaluate the performance of this full reconstruction attack?

Unique Challenges and Strategies Beyond the challenges previously discussed, the feasibility of gradient-based GU-FGRA under realistic attack settings remains underexplored. Since no shadow graphs or models are available and only minimal prior knowledge is mastered, even a simple unlearning attack targeting a single node is an intricate task. Notably, our goal is to reveal full unlearned graphs rather than a simple

combination of multiple attribute inference attacks of the removed node and multiple link membership inference attacks of its 1-hop neighbors. This challenge is further exacerbated under multiple-node removal, where more complex structural and feature entanglements yield increasingly ambiguous gradient proxies for full graph recovery.

To answer the key research questions and to address their unique challenges under realistic white-box settings, we present **GraphToxin, the first full graph reconstruction attack against graph unlearning**. Since the difference between publicly accessible gradients of the original and unlearned GNNs implicitly captures the information associated with the unlearned graph, GraphToxin exploits this difference for full graph recovery through three core modules. First, a gradient matching module acts as a holistic roadmap for full unlearned graph recovery by bridging the gap between the ground-truth gradient difference and the gradients generated from the recovered unlearned graph, however, it only yields a coarse proxy. Second, a novel curvature matching module provides fine-grained signals by downweighting the directions of high curvature to ultimately produce a more plausible recovery solution. Finally, a feature smoothness module is utilized to enforce similarity among connected nodes.

GraphToxin also tackles the intractable challenge of the data-free black-box setting. This scenario presents a major hurdle since the adversary is restricted to using only the model’s posterior probabilities instead of its gradients. This limitation inevitably introduces approximation errors, as black-box GU-FGRA must attempt to infer fine-grained graph details from coarse posterior outputs, which can degrade the reconstruction quality. To mitigate this issue, GraphToxin introduces a semantic calibration module. The goal of this module is to minimize the discrepancy between the ground-truth labels and the predictions for the recovered nodes, thereby encouraging semantically consistent reconstructions.

The effectiveness of GraphToxin is evaluated through a comprehensive evaluation framework. Existing GU methods primarily focus on small-scale random removals, which provides an incomplete assessment of reconstruction risks. [3, 21, 41, 43]. Given the inherent sparsity of real-world graphs, this operation often selects nodes that are less influential for model predictions. These “unimportant” nodes typically possess low degrees and cause negligible influences after removal. However, in reality, attackers would prioritize high-value targets. To better mimic actual attacks, we propose a worst-case evaluation. In our work, we define this worst-case scenario as the removal of the top 10% of nodes with the highest degrees. Furthermore, traditional evaluation metrics are often insufficient to characterize reconstruction quality [7, 34, 50]. Motivated by this limitation, we develop a systematic evaluation framework that incorporates reconstruction-related metrics to capture the global consistency of recovered features and topology, and performance-level metrics to assess functional utility of the full recovered graph.

Contribution Our contributions are summarized as follows:

1. **Pioneering Attack:** We design GraphToxin, the first full graph reconstruction attack against graph unlearning. It not only recovers the removed nodes and their graph topology, but also steals the sensitive information of their neighbors, posing more detrimental privacy risks.
2. **Novel Methodology:** We propose a novel curvature matching module to provide fine-grained guidance for full unlearned graph recovery in realistic settings.
3. **Scalability and Generalization:** We successfully extend GraphToxin to multiple-node removal with comparable attack performance, and generalize GraphToxin to the black-box setting with only minimal prior knowledge.
4. **Rigorous Evaluation Framework Design:** We propose a comprehensive evaluation framework grounded in feature-level, global-level, and performance-level perspectives. Additionally, we assess GraphToxin after removing the most influential nodes to assess its attack potency in reality.
5. **Empirical Validation:** We conduct extensive experiments across diverse graph datasets, GNN backbones, and both exact and approximate graph unlearning methods. The results demonstrate the effectiveness and flexibility of GraphToxin in both white-box and black-box settings, for single or multiple-node removal.
6. **Highlighting Urgency for Robust Defenses:** We empirically show that existing defense methods are ineffective against GraphToxin and in some cases may even amplify its attack performance. This finding highlights the urgent need for developing more effective defense mechanisms against this potent attack.

Social Impacts GraphToxin is significantly more detrimental than existing inference attacks, particularly in high-stake scenarios, because it recovers not only an individual’s sensitive content and personal links, but also confidential information of her/his contacts. For instance, in financial crediting, revealing the full unlearned transaction graphs can expose private trades and confidential documents; in healthcare management, reconstructing full health information can fuel workplace discrimination, insurance denial, or social stigma. Once privacy is undermined, the consequences are twofold: first, it can trigger a cascade of adversarial attacks, such as re-identification or model extraction; second, organizations face liability for non-compliance with regulations and simultaneously erode users’ trust in their AI systems.

2 Background and Problem Statement

2.1 Notations

Given an undirected attributed graph $\mathcal{G} = (\mathcal{V}, \mathcal{E}, X)$, \mathcal{V} denotes the set of nodes with $|\mathcal{V}|$ elements and each node v is

associated with a feature vector $X_v \in \mathbb{R}^{1 \times d}$ and a label vector $Y_v \in \mathbb{R}^{1 \times |\mathcal{Y}|}$, where d is the feature dimensionality and $|\mathcal{Y}|$ denotes the number of labels. \mathcal{E} denotes the set of edges with $|\mathcal{E}|$ elements, which can be represented by an adjacency matrix $A \in \{0, 1\}^{|\mathcal{V}| \times |\mathcal{V}|}$, where $A_{w,v} = 1$ iff $(w, v) \in \mathcal{E}$, and $A_{w,v} = 0$ otherwise. For simplicity, we denote the graph as $\mathcal{G} = (A, X)$. \mathcal{F}_o , \mathcal{F}_u and \mathcal{F}_a indicate the original GNN, unlearned GNN, and attack model, respectively.

2.2 Graph Neural Networks

The exceptional performance of most GNNs stems from the message-passing mechanism, which aggregates information from each node v ’s local neighborhood $\mathcal{N}(v)$ and iteratively updates the node embedding H_v^k after k layers. Formally, this process can be expressed as:

$$H_v^k = \text{UPD}^k(H_v^{k-1}, \text{AGG}^{k-1}(\{H_w^{k-1} : w \in \mathcal{N}(v)\})) \quad (1)$$

where $H_v^0 = X_v$, and UPD and AGG are two arbitrary differentiable functions to design diverse GNN variants. For node classification tasks, generally, H_v^k is fed into a linear classifier with a softmax function for final prediction.

2.3 Graph Unlearning

We consider the most challenging GU—node unlearning throughout our paper, which is formally defined as:

Definition 1 (Single Node Unlearning). Given the original training graph $\mathcal{G} = (A, X)$, the original trained GNN \mathcal{F}_o and a single unlearning request $\Delta\mathcal{G}_v = (v, \mathcal{E}_{\mathcal{N}^1_v}, X_v)$, node unlearning aims to unlearn a single node v , its feature X_v and its links to 1-hop neighbors \mathcal{N}_v^1 by training an unlearned model \mathcal{F}_u on the remaining graph $\mathcal{G} \setminus \Delta\mathcal{G}_v$ that approximates the fully retrained model $\mathcal{F}_o'(\mathcal{G} \setminus \Delta\mathcal{G}_v)$.

Definition 2 (Multiple Node Unlearning). Upon receiving multiple unlearning requests $\Delta\mathcal{G} = (\mathcal{V}_M, \mathcal{N}_M^1, X_M)$, node unlearning aims to unlearn multiple nodes \mathcal{M} , their node features X_M and links to their 1-hop neighbors \mathcal{N}_M^1 by training unlearned model \mathcal{F}_u on the remaining graph $\mathcal{G} \setminus \Delta\mathcal{G}$ that approximates the fully retrained model $\mathcal{F}_o'(\mathcal{G} \setminus \Delta\mathcal{G})$.

2.4 Graph Reconstruction Attack (GRA)

Definition 3 (General GRA). Given access to a GNN \mathcal{F}_o trained on graph \mathcal{G} , a GRA \mathcal{F}_a endeavors to recover sensitive information \mathcal{G}_{par} that is indistinguishable from its ground-truth information $\mathcal{G}_{par} \in \mathcal{G}$.

Depending on the adversary’s interaction with \mathcal{F}_o , a general GRA reduces to a white-box setting when the adversary can access model gradients $\nabla \mathcal{L}(\theta)$ (hereinafter abbreviated as $\nabla \mathcal{L}$), where θ denotes model parameters. Under the gray-box setting, GRA allows the adversary to access intermediate

model outputs such as node embeddings but no gradient-level information, whereas the black-box setting restricts the adversary to only query the victim model, without access to internal representations or gradients.

Based on the recovered information \hat{G}_{par} , a general GRA can be instantiated to target different graph components. Specifically, it can recover partial or complete node features via attribute inference attacks, infer the existence of specific edges through link stealing attacks, or reconstruct structural information via graph topology reconstruction attacks. In this work, we focus on the most challenging setting, namely full GRA, which aims to jointly recover both full node features and graph topology of the target graph. A systematic comparison of these attack paradigms is provided in Table 1.

2.5 Problem Statement

We formally define the full graph reconstruction attack against graph unlearning (GU-FGRA). Specifically, for single-node removal, a GU-FGRA aims to recover the full unlearned graph $\mathcal{G}_{u_v} = (\mathcal{V}_{u_v}, \mathcal{E}_{u_v}, X_{u_v})$, where the recovered nodes $\mathcal{V}_{u_v} = [v, \mathcal{N}_v^1]$ contain the removed node v and its affected 1-hop neighbors \mathcal{N}_v^1 . Please note that $\mathcal{G}_{u_v} \neq \Delta\mathcal{G}_v$. Unlike $\Delta\mathcal{G}_v$, \mathcal{G}_{u_v} additionally recovers node features of its 1-hop neighbors. Moreover, recovering $\Delta\mathcal{G}_v$ can be simply treated as a combination of d times attribute inference attacks of a single node v and a graph topology reconstruction attack of its associated links \mathcal{N}_v^1 , where d denotes the number of node features. In contrast, recovering \mathcal{G}_{u_v} is significantly more complicated, as it further requires the simultaneous full feature recovery of multiple recovered nodes. For multiple-node removal, attackers strive to reconstruct $\mathcal{G}_u = (\mathcal{V}_u, \mathcal{E}_u, X_u)$. Similarly, $\mathcal{G}_u \neq \Delta\mathcal{G}$ where $\mathcal{V}_u = [\mathcal{V}_M, \mathcal{N}_M^1]$ contains multiple removed nodes M and their 1-hop neighbors \mathcal{N}_M^1 . Under white-box settings, the adversary leverages model gradients $\nabla\mathcal{L}$ to recover the full unlearned graph for both single-node or multiple-node removal, while under black-box settings, she/he exploits the posterior probabilities $P = (p_1, p_2, \dots, p_{|\mathcal{Y}|})$ obtained before and after node removals to achieve the same objective.

3 Attack Framework Design

In this section, we formalize the threat model and introduce GraphToxin, the first data-free full graph reconstruction attack against graph unlearning, followed by an evaluation framework to systematically assess it.

3.1 Threat Model

3.1.1 Attacker’s Goal

The attacker aims to fully reconstruct the unlearned graph, including the removed nodes, their affected neighborhoods, the induced topological structures, and associated node features.

3.1.2 Attacker’s Knowledge and Capabilities

We consider a standard MLaaS deployment involving a model owner, a server, and users. The model owner trains a GNN on a private graph and uploads the GNN to the server. The server then deploys the model and packs it into an API for users to use [2, 15]. Upon receiving an unlearning request from a participant (i.e., a specific node in the private training graph), the model owner adopts a graph unlearning method to remove any information associated with that participant (i.e., its node features and neighboring links), releases the unlearned GNN, and deletes the previous version. However, the involvement of multiple parties and time gaps between model updates expand the attack surface, where the adversary can exploit to reconstruct the full unlearned graphs in a data-free manner.

Our attack setting fundamentally differs from existing reconstruction attacks. They assume that the adversary either has partial access to the original training graphs or unlearned graphs, or can obtain shadow graphs. However, these assumptions are unrealistic: first, original training graphs are proprietary and constitute valuable assets of companies and institutions, necessitating strong protections against potential attackers; second, shadow graphs typically demand same or similar distributions from the original training graphs. Since training graphs are usually protected, it is hard for the adversary to acquire the distribution information. Therefore, GU-FGRA should be strictly operated under a data-free setting.

We consider two types of attackers: the honest-but-curious server and malicious user. Following Hu et al., [15], the server has the white-box access to the original and unlearned GNNs, but only restricted to model gradients, without any prior knowledge of unlearning methods, GNN architecture, and training or unlearned graph distributions. This assumption is realistic as the server can save copies of all uploaded models or archive the deleted versions for legitimate reasons, including but not limited to backup, auditing, debugging, or rollback after accidental deletion. Meanwhile, the malicious user only has the black-box access to the original and unlearned GNNs. She/he can submit model queries to the server, and the server will faithfully respond these queries and send posterior-based model predictions back. The user can conduct data-free model stealing attacks to construct surrogate models based on collected query-response pairs [54]. In addition, auditors can also act as a red team to launch GU-FGRA with only the minimal required knowledge in a data-free setting, enabling them to discover vulnerabilities and anomalies to improve the security and privacy of graph-based AI systems.

We assume that the adversary has knowledge of the number of removed nodes and edges, as well as changes in label distributions. This assumption is practical since such information can be exposed through simple count queries, system logs or publicly available technical documents, which are commonly provided on MLaaS platforms to facilitate proper model usage. Moreover, attackers can employ existing label inference

Table 1: **Attack Comparison.** \checkmark represents “access” or “applicable”, and \emptyset denotes “not applicable” or “unknown”. N/A means currently unexplored in the field.

Attack Type	Attacker’s Knowledge and Capabilities			Recovery Content		Attack Unlearning Case	
	Graph Data	Model Access	Graph Unlearning	Feature	Topology	Random	Worse
Attribute Inference Attack (N/A)	Partial/Shadow Graph	Grey/Black Box	\emptyset	Single/Partial	\emptyset	\emptyset	\emptyset
Link Stealing Attack [46]	Partial/Shadow Graph	Grey/Black Box	Partial Unlearned Graph	\emptyset	Single Edge	\checkmark	\emptyset
Graph Topology Reconstruction Attack (N/A)	Partial/Shadow Graph	Grey/Black Box	\emptyset	\emptyset	Partial/Full	\emptyset	\emptyset
Full Graph Reconstruction Attack (Ours)	Data-free	White/Black Box	#of Node/Edge/Label Changes	Full	Full	\checkmark	\checkmark

techniques to recover labels, which serve as a cornerstone for subsequent reconstruction attacks [10, 15].

3.2 Attack Framework Design

We introduce GraphToxin and present its framework overview in Figure 1. GraphToxin contains three modules: *Gradient Matching* to extract holistic information for the full unlearned graph recovery, *Curvature Matching* to provide more fine-gradient recovery signals and *Feature Smoothness* to capture and enforce similarity among connected nodes within the unlearned graph. We detail each module as follows.

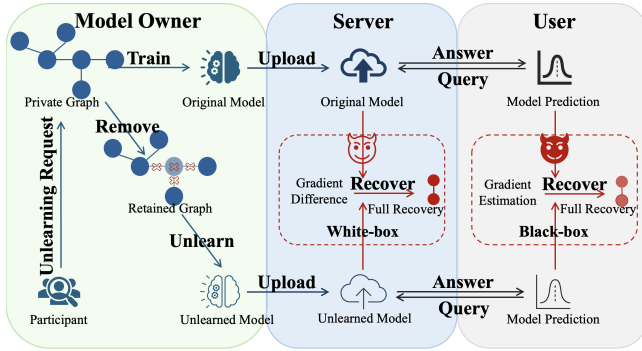


Figure 1: An overview of GraphToxin. The white-box GraphToxin uses gradient difference for full unlearned graph recovery. The black-box GraphToxin first estimates gradients and then exploits their difference for recovery.

3.2.1 Gradient Matching

Design Rationale Gradient matching is the foundation of gradient inversion attacks mainly tailored for federated learning. Given the gradients with respect to model parameters, gradient matching first initializes a dummy input and then iteratively optimizes it by minimizing the distance between the gradients induced by the dummy input and the observed model gradients. Since our attack settings are strictly data-free and only assume the adversary access to actual or estimated gradients of the original and unlearned models, gradient matching serves as a natural starting point.

In the graph domain, gradient matching searches for a candidate graph whose induced gradients are consistent with

the observed ones. Rather than assuming a direct correspondence between gradients and individual graph components, this process imposes a constraint that narrows the space of plausible graph reconstructions. However, gradient matching cannot be trivially applied to GU-FGRA, as the attack involves two gradient sets from the original and unlearned models. Naively applying gradient matching to each gradient set introduces redundant optimization paths while discarding the unlearning-induced discrepancy that carries the most informative recovery signals. Due to the ambiguity of gradient-to-graph mappings, independently reconstructed graphs are not guaranteed to align, hindering the reliable identification of unlearned graph components.

These limitations motivate a discrepancy-driven design that directly operates on gradient differences between the original and unlearned GNNs, rather than on separate gradient sets.

Gradient Matching in GU-FGRA For clarity, we begin with the single-node removal setting and discuss the extension to multiple-node removal in a separate section.

Formally, let $\nabla \mathcal{L}$ and $\nabla \mathcal{L}^{-v}$ denote the gradients of the original and unlearned GNNs, respectively, where $-v$ represents an unlearning request on a single node v . We define the observed gradient difference as $\Delta \nabla \mathcal{L} = \nabla \mathcal{L} - \nabla \mathcal{L}^{-v}$, which captures unlearning-induced signals associated with the removed node v and its affected neighborhoods \mathcal{N}^1_v . The adversary first initializes a dummy graph with the fixed unlearning graph size, and then optimizes it by minimizing the distance between the dummy and observed gradient difference to recover the full unlearned graph $\mathcal{G}_{u_v} = (\mathcal{V}_{u_v}, \mathcal{E}_{u_v}, \mathcal{X}_{u_v})$, where $\mathcal{V}_{u_v} = [v, \mathcal{N}^1_v]$. The attack objective is represented as:

$$\tilde{\mathcal{G}}_{u_v} = \arg \min_{\tilde{\mathcal{G}}_{u_v}} \mathcal{D}(\Delta \tilde{\nabla} \mathcal{L}, \Delta \nabla \mathcal{L}) \quad (2)$$

where $\Delta \tilde{\nabla} \mathcal{L}$ denotes the gradients induced by the dummy graph. For the choice of the distance function \mathcal{D} , existing gradient matching commonly uses cosine similarity [11, 15] or L2 distance [53]. Some prior studies favor L2 distance for its superior attack performance while others [22] show that cosine similarity correlates more strongly with reconstruction quality. Inspired by Fan et al. [9], we combine both metrics to leverage their complementary strengths. Specifically, we adopt Mean Squared Error (MSE), a normalized form of L2 distance, to penalize the absolute deviations and mitigate the influence of magnitude amplification in the high-dimensional gradient space. Meanwhile, cosine similarity is used for direction consistency and semantic alignment. Following Fan

et al. [9], we treat these two losses equally:

$$\mathcal{L}_{grad} = 1 - \frac{\langle \Delta \tilde{\nabla} \mathcal{L}, \Delta \nabla \mathcal{L} \rangle}{\|\Delta \tilde{\nabla} \mathcal{L}\| \cdot \|\Delta \nabla \mathcal{L}\|} + \frac{1}{M} \sum_{i=1}^M ((\Delta \tilde{\nabla} \mathcal{L})_i - (\Delta \nabla \mathcal{L})_i)^2 \quad (3)$$

where M is the number of elements in the gradients.

3.2.2 Curvature Matching

Motivation Gradient matching provides holistic information for the full unlearned graph recovery, however, it is not sufficient to extract more fine-grained recovery signals. The following illustrative example demonstrates how gradient matching leads to ambiguity in GU-FGRA and motivate the design of curvature matching.

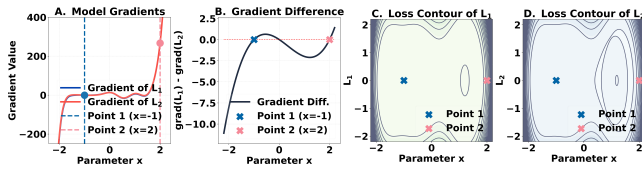


Figure 2: Example of the Ambiguity of Gradient Matching

As depicted in Figure 2, we consider a convex loss function \mathcal{L}_1 and obtain \mathcal{L}_2 by adding noises and slightly changing the polynomial coefficients of \mathcal{L}_1 to simulate the effect of unlearning. As shown in Fig. 2.A and B, the two losses induce nearly identical gradients and small gradient difference. However, we identify two distinct points (marked in blue and pink) that produce the identical gradient difference, yet exhibit the substantially different curvatures of the loss landscape as shown in Fig. 2.C and D. This example highlights a fundamental limitation of gradient matching: multiple candidates can satisfy the same gradient difference constraint. In graph learning, this ambiguity is further amplified by the permutation invariance of GNNs, under which different graph structures can yield identical information propagation and gradients. Moreover, GU-FGRA aims to recover not only the removed node and its incident edges, but also the features of affected neighboring nodes. While gradient difference can reflect the removal of a node and local connectivity changes, they impose insufficient constraints to uniquely characterize neighboring node features. To overcome this ambiguity and provide fine-grained signals for full unlearned graph recovery, we next introduce a novel curvature matching module.

Curvature Matching in GU-FGRA We formalize curvature matching as a curvature-aware constraint operating on gradient difference. Detailed theorem assumptions and proof are provided in Appendix A.

Theorem 1 (Curvature-aware difference Matching). *Under standard smoothness and local approximation assumptions, minimizing the gradient difference reduces to*

minimizing the curvature-weighted difference $(\Delta \tilde{\nabla} \mathcal{L} - \Delta \nabla \mathcal{L})^T H^{-1}(\Delta \tilde{\nabla} \mathcal{L} - \Delta \nabla \mathcal{L})$.

In practice, the Hessian matrix H is computationally infeasible as it requires calculating and storing second-order derivatives. We leverage the Fisher Information Matrix F as the surrogate. Specifically, F is defined as the covariance matrix of the gradient of the log-likelihood function with respect to model parameters θ , quantifying the sensitivity of the model’s predicted probability distribution to small changes in θ . According to Rame et al. [29], F approximates H with probably bounded errors under regular conditions. However, since the full F involves an expectation over all possible outputs, the empirical Fisher Information \tilde{F} is typically utilized as an efficient approximation [17]. Formally, \tilde{F} is denoted as:

$$\tilde{F} = \frac{1}{N_u} \sum_{i=1}^{N_u} (\nabla \log p(Y_i | \tilde{G}_u, \theta)) (\nabla \log p(Y_i | \tilde{G}_u, \theta))^T \quad (4)$$

where $N_u = |\mathcal{V}_u|$ is the node size of \mathcal{G}_u .

We then replace H with \tilde{F} in $(\Delta \tilde{\nabla} \mathcal{L} - \Delta \nabla \mathcal{L})^T H^{-1}(\Delta \tilde{\nabla} \mathcal{L} - \Delta \nabla \mathcal{L})$ and derive the following curvature matching loss:

$$\mathcal{L}_{curv} = (\Delta \tilde{\nabla} \mathcal{L} - \Delta \nabla \mathcal{L})^T \tilde{F}^{-1} (\Delta \tilde{\nabla} \mathcal{L} - \Delta \nabla \mathcal{L}) \quad (5)$$

\mathcal{L}_{curv} naturally encodes the curvature of the loss landscape, providing more fine-grained signals for full unlearned graph recovery. Not all gradient difference are equally informative: some may stem from noises or redundant parameterization, while others are highly indicative of the ground-truth features and underlying graph structures. By incorporating \tilde{F} , \mathcal{L}_{curv} downweights the directions of high curvature, thereby biasing the optimization toward smoother and more stable directions in parameter space. Furthermore, \tilde{F} is defined with respect to model predictions and thus implicitly reflects how node features and graph structures are propagated through message passing and projected into posterior probabilities. This complementary perspective provides sensitivity-aware guidance that better aligns with the model’s local behavior.

3.2.3 Feature Smoothness

Most real-world graphs follow the homophily principle, where neighboring nodes tend to share similar features. Graph Dirichlet energy [16, 46, 50] explicitly captures and quantifies this feature smoothness:

$$\mathcal{L}_{smooth} = \text{tr}(X^T L X) \quad (6)$$

where tr is the trace of a matrix, $L = D - A$ is the laplacian matrix and D is the diagonal degree matrix.

This regularization penalizes sharp feature differences across connected nodes and suppresses degenerate and noisy solutions for realistic full graph recovery.

3.2.4 Loss Function

In summary, the final objective of GraphToxin is:

$$\mathcal{L}_{white} = \mathcal{L}_{grad} + \alpha_1 \mathcal{L}_{curv} + \alpha_2 \mathcal{L}_{smooth} \quad (7)$$

where α_1 weights the curvature-aware loss while α_2 controls feature smoothness regularization. We refer to them as the Fisher coefficient and the Laplacian coefficient, respectively.

3.3 Extensions: Multiple-Node Removal and Black-box GraphToxin

3.3.1 Multiple-Node Removal

For multiple-node removal, the topology of the full unlearned graph \mathcal{G}_u is significantly more complex due to the interconnection of removed nodes and their affected neighbors.

To simultaneously reconstruct node features and such more complicated graph topology, we first initialize the topological structure by sampling a fixed number of edges using Bernoulli distribution [34], marked as $\tilde{A}_0 \sim Bernoulli(p)$, where $p = \frac{|\mathcal{E}_u|}{\binom{|\mathcal{V}_u|}{2}}$ controls the expected edge density and aligns with the known edge budget. Next, we adopt the same final objective \mathcal{L}_{white} as in the single-node removal case, while additionally updating the adjacency matrix \tilde{A} via projected gradient descent [34]. Each entry (i, j) of \tilde{A} is updated through the entry-wise projection operator as:

$$\hat{A}_{ij} = \text{proj}_{[0,1]}(\tilde{A}_{ij}) = \begin{cases} 1, & \tilde{A}_{ij} \geq 1 \\ 0, & \tilde{A}_{ij} \leq 0 \\ \tilde{A}_{ij}, & \text{otherwise} \end{cases} \quad (8)$$

We then repeat the sampling process using the learned edge probabilities from the last iteration to generate the final reconstructed adjacency matrix \hat{A} .

3.3.2 Black-box GraphToxin

Distinct from the white-box setting, black-box GraphToxin cannot access gradients and relies solely on posterior probabilities. Despite this constraint, the attack remains feasible in practice. The adversary first obtains surrogate models of the original and unlearned GNNs (\mathcal{F}_o' and \mathcal{F}_u') via an existing data-free, black-box model extraction attack [54]. We refer the interested readers to [54] for additional details.

Once the copycats are stolen, GraphToxin exploits the gradient difference between these copycats using the same objective \mathcal{L}_{white} for full unlearned graph recovery. However, the reconstruction quality highly depends on the stealing quality. Imperfect model extraction may introduce additional noise into the estimated gradients. We incorporate a semantic calibration loss to mitigate this effect:

$$\mathcal{L}_{seman} = CE(\tilde{Y}_u, Y_u) = - \sum_{i=1}^{|\mathcal{V}_u|} Y_{u_i} \cdot \log p_{u_i} \quad (9)$$

where CE is the cross-entropy loss to minimize the discrepancies between the actual node labels and the model predictions of the dummy graph $\tilde{\mathcal{G}}_u$ from the copycat \mathcal{F}_o' .

The final objective for black-box GraphToxin is:

$$\mathcal{L}_{black} = \mathcal{L}_{grad} + \alpha_1 \mathcal{L}_{curv} + \alpha_2 \mathcal{L}_{smooth} + \alpha_3 \mathcal{L}_{seman} \quad (10)$$

where α_3 controls the contribution of semantic calibration, referred as the calibration coefficient.

3.4 Evaluation Framework Design

3.4.1 Worst-case Scenario

Existing graph unlearning studies evaluate unlearning effectiveness under random node removals, but fail to examine worst-case scenarios where highly influential nodes are removed. These scenarios serve as a stress test rather than a favorable condition for the attack. Removing influential nodes indeed induces larger parameter changes, while simultaneously increases reconstruction difficulty. Such nodes typically possess high degrees, amplifying multi-hop dependencies and thereby complicating the attribution of entangled features and topologies. Moreover, worst-case settings align with realistic attacker incentives. Nodes with high influence, such as public figures in a social network, are more likely to trigger unlearning requests and may attract stronger attack interests than normal users.

For single-node removal, we unlearn the top 10% nodes with the highest degrees from the training graph and report their average attack results to assess the worst-case scenarios, while in multiple-node removal, the top 25, 50, 75 nodes with the highest degrees are selected and partitioned into 5 non-overlapping pairs based on their degree ranking.

3.4.2 Feature-level Evaluation

Feature-level evaluation measures the quality of node attributes within the recovered unlearned graph $\tilde{\mathcal{G}}_u$.

Root Normalized Mean Squared Error (RNMSE) We follow Sinha et al. [34] and leverage RNMSE to quantify the discrepancies between the recovered and actual node features.

$$\text{RNMSE}(\tilde{X}_v, X_v) = \frac{\|\tilde{X}_v - X_v\|}{\|X_v\|} \quad (11)$$

We finally report the average RNMSE of all nodes in $\tilde{\mathcal{G}}_u$. While RNMSE is a standard metric for feature recovery, it does not fully capture structural similarity or functional consistency, as we empirically demonstrate in Section 4.3.1.

3.4.3 Global-level Evaluation

Global-level evaluation assesses the preservation of joint feature-topology structure of the recovered unlearned subgraph.

We assume that the adversary knows the size of the full unlearned graph. For single-node removal, the graph topology is fixed, and thus topology-level evaluation is unnecessary. For multiple-node removal, traditional link-wise reconstruction metrics like Area under Curve (AUC) and Average Precision (AP) fail to capture holistic structural patterns. Therefore, we adopt the following global-level evaluation metrics:

Embedding Distance (ED) Node embeddings encode both node features and multi-hop structural patterns. Consequently, we measure the similarity between the embeddings of the recovered and ground-truth unlearned graphs, which are both extracted from the original GNN model, denoted as \tilde{H}^k, H^k , respectively. Here, k is the number of GNN layers, usually $k = 2$. We leverage the squared quadratic Wasserstein distance ($p=2$) [36] to quantify this similarity, defined as $ED = W_2^2(\tilde{H}^k, H^k)$.

Pyramid Match Graph Kernel (PMGK) PMGK is a robust measure for graph matching [25], which captures structural similarity across multiple scales. Specifically, we first discretize continuous node embeddings of the recovered and ground-truth graphs into a set of discrete labels via K-means clustering, thereby grouping nodes with similar structural or semantic patterns. We then create a multi-resolution histogram of these labels of each graph and then take a weighted sum of the intersections of these two histograms. In our experiment, PMGK is computed using the grakel library [33].

3.4.4 Performance-level Evaluation

Performance-level evaluation examines whether the recovered unlearned graph is functionally equivalent to the full unlearned graph when processed by the same GNN. This level of evaluation is essential as feature and structural similarities alone cannot guarantee the similar model behavior.

Attack Accuracy (ATT. ACC) Attack accuracy measures whether the recovered graph leads to the same predicted labels as the ground-truth unlearned graph under the same GNN.

$$ATT.ACC = \frac{1}{|\mathcal{V}_u|} \sum_{v \in \mathcal{V}_u} \mathbb{I} \left[\arg \max \tilde{p}_v = \arg \max p_v \right] \quad (12)$$

where $\mathbb{I}[\cdot]$ is the indicator function and p is the posterior probability produced by the original GNN \mathcal{F}_o .

Attack Fidelity (ATT. FID) Attack fidelity quantifies how accurately the recovered graph reproduces the model-specific predictions of the full ground-truth unlearned graph.

$$ATT.FID = \frac{1}{|\mathcal{V}_u|} \sum_{v \in \mathcal{V}_u} \mathbb{I} \left[\arg \max \tilde{p}_v = \arg \max \hat{p}_v \right] \quad (13)$$

where \hat{p}_v denotes the posterior probability vectors produced by the original GNN on the ground-truth unlearned graph.

Posterior Wasserstein Distance (PWD) To further capture the confidence alignment at the distribution level, we measure the distance between posterior distributions induced by the recovered and ground-truth unlearned graphs using the squared quadratic Wasserstein distance as $PWD = W_2^2(\tilde{p}, \hat{p})$.

4 Experimental Validation

In this section, we conduct empirical experiments across a range of GNN variants, graph unlearning methods and graph datasets to answer our three primary research questions. Specifically, we investigate the following key subquestions:

- SQ1:** Why is comprehensive evaluation necessary?
- SQ2:** How GraphToxin performs for single-node removal?
- SQ3:** Can GraphToxin flexibly adapt to different graph unlearning methods and GNN backbones?
- SQ4:** How GraphToxin performs in worst-case scenarios?
- SQ5:** Which impact factors dominate GraphToxin?
- SQ6:** How GraphToxin performs in multiple-node removal?
- SQ7:** Can GraphToxin be extended to the black-box setting?
- SQ8:** How resilient is GraphToxin against defenses?

4.1 Setups

4.1.1 Datasets

We conduct experiments on three benchmark graph datasets: Cora, PubMed [44], and Amazon-Photo (Photo) [32]. Dataset details are provided in Appendix B.1.

4.1.2 Unlearning Methods

We consider the following graph unlearning methods. (1) Exact unlearning: We directly retrain the GNNs from scratch (Retraining). (2) Approximate unlearning: We consider two state-of-the-art graph unlearning methods with distinct frameworks: MEGU [21] and ETR [43]. MEGU is a learning-based method that employs predictive and unlearning modules to mitigate unlearning effects, while ETR is a training-free method designed to erase the influence of deleted nodes and rectify the collateral damage to their neighbors.

The original training and graph unlearning results across different GNN backbones and graph datasets are detailed in Table 5 in Appendix B.3, which confirm the effectiveness of all considered graph unlearning methods.

4.1.3 GNN Variants

We use three classical GNN backbones: GCN [18], GraphSAGE [12] and SGC [40].

4.1.4 Baselines

To the best of our knowledge, GraphToxin is the first GU-FGRA, there are no established baseline methods for direct comparison. Accordingly, we consider the following alternative baselines: (1) Random Graph (Rand.), which generates random graphs using Gaussian noise without parameter updates. (2) Learning with A Few Epochs (FewE.), which trains GraphToxin for only the first 1% of the total training epochs. This baseline represents a weak attacker with severely

limited optimization budget. Direct adaptations of gradient inversion attacks (i.e., gradient matching alone) are evaluated as ablations (Please see Section 4.3.4) rather than standalone baselines, as they represent simplified variants of GraphToxin.

4.1.5 Implementation

All experiments are implemented on 4 Nvidia A100 GPUs. For implementation details, please refer to Appendix B.2.

4.2 Attack Performance (SQ1 - SQ3)

4.2.1 Necessity of Comprehensive Evaluation (SQ1)

We first examine the necessity of worst-case evaluation. From Table 2, we observe that averaging results under random node removal can obscure meaningful differences in reconstruction difficulty, motivating the need for worst-case evaluation. PubMed exemplifies this problem. Due to its high sparsity and limited label space, a random node removal often produces relatively simple recovery targets, under which even randomly generated graphs may achieve seemingly strong performance-level scores. This effect can artificially inflate average performance and mask the weakness of Rand. on more complex unlearning instances. In contrast, under the worst-case settings, the performance of Rand. significantly decreases, while GraphToxin remains effective, providing a more faithful assessment of reconstruction attacks under challenging unlearning scenarios.

We subsequently motivate a comprehensive evaluation framework for GU-FGRA. Existing attacks commonly rely on RNMSE for assessing feature reconstruction quality [34]. While RNMSE is a standard and necessary metric, it is insufficient when used in isolation. Table 2 shows that even a randomly generated graph may achieve a relatively low RNMSE while performing poorly on performance-level metrics. This discrepancy indicates that RNMSE alone can obscure qualitative differences between the recovered and ground-truth unlearned graphs, which are further amplified by the message-passing paradigm in GNNs. Hence, more sensitive metrics are required to discern subtle variations. Specifically, when RNMSE values are nearly indistinguishable, ED can reveal substantial divergence in the joint feature–structure space. Furthermore, since single-node removal typically induces only subtle parameter changes, reconstruction results across different unlearning methods yield distinct values yet appear nearly identical on the scale of $1e-2$. In contrast, PMGK can reflect fine-grained changes that are imperceptible to other metrics.

4.2.2 Effectiveness (SQ2)

As shown in Table 2, GraphToxin consistently and substantially outperforms baselines across *all* experimental settings on nearly every reconstruction quality and performance-level

evaluation metrics. The superiority of GraphToxin generalizes across diverse graph datasets and graph unlearning methods. In addition, GraphToxin’s overall advantage holds under both random and worst-case node removal scenarios, highlighting its robustness. On performance-level metrics, GraphToxin achieves up to **11.14**× improvement over Rand. on Cora, and up to **86.73**× on Photo.

4.2.3 Flexibility (SQ3)

We evaluate the flexibility of GraphToxin across different graph unlearning methods and GNN backbones.

Graph Unlearning The results in Table 2 demonstrate the stable and consistent performance of GraphToxin across *all* graph unlearning methods. While minor variations are observed, these differences arise from the interaction between how unlearning signals are manifested in the parameter space and the structural properties of the underlying graphs. Specifically, the attack against Retraining tends to induce larger parameter changes, which are particularly exploitable in small and sparse graphs such as Cora. In contrast, MEGU introduces learning-based modules to suppress large parameter deviations. This design mitigates the propagation of unlearning signals and can lead to reduced distinguishability under structure-sensitive metrics such as PMGK. ETR adopts a training-free and highly localized strategy that erases the influence of deleted nodes while rectifying collateral damage to neighboring nodes. Therefore, ETR can better preserve local structures, which may account for its stronger global-level alignment across diverse graphs.

GNN Backbones We next fix the unlearning target as Retraining and investigate the impact of different GNN backbones. Compared to the nearly identical performance observed across unlearning methods in Table 2, *GraphToxin exhibits distinct performance across GNN backbones, while still maintaining its overall superiority and generalization across all graph datasets* (Table 6). Detailed results and analysis are provided in Appendix B.4 due to space constraints.

4.3 Parameter Studies (SQ4 and SQ5)

4.3.1 Worst-case Analysis

Previous subsections motivate the necessity of worst-case evaluation. We now analyze its impact on attack performance. As summarized in Table 2 and Table 6, worst-case node removal leads to markedly different behaviors across graphs. On Cora, GraphToxin consistently achieves stronger performance under worst-case removal across nearly all metrics, except PMGK. In contrast, on PubMed and Photo, GraphToxin generally performs better under random-node removal for global and performance-level metrics. Similar trends are observed across different GNN backbones.

This divergence highlights the inherent trade-off in worst-case evaluation. Removing high-degree nodes increases re-

Table 2: **The Performance of GraphToxin for single-node Removal (Backbone: GCN).** Unit: **1e-2**. Arrow indicates the direction of better performance and the **blue** color denotes the superb ‘best’ results (in **bold**).

Dataset	GU	Baseline	RNMSE(\downarrow)		ED(\downarrow)		PMGK(\uparrow)		ATT. ACC(\uparrow)		ATT. FID(\uparrow)		PWD(\downarrow)	
			Random	Worst	Random	Worst	Random	Worst	Random	Worst	Random	Worst	Random	Worst
Cora	Retrain	Rand.	6.59	3.61	78.76	72.45	84.35	68.35	6.79	9.18	6.31	7.48	82.79	80.23
		FewE	5.08	2.84	73.11	65.96	84.62	68.79	57.50	39.29	56.67	37.98	40.47	56.30
		Toxin	4.11	1.95	71.38	52.35	84.05	67.21	72.21	84.72	69.00	77.97	29.66	22.35
	MEGU	Rand.	6.59	3.61	78.76	72.45	84.19	68.64	6.79	9.18	6.31	7.48	82.79	80.23
		FewE	5.08	2.84	73.16	66.02	84.11	67.73	57.50	39.29	56.67	37.98	40.48	56.31
		Toxin	4.23	2.10	71.84	51.18	84.30	67.21	71.14	82.22	70.31	77.85	30.22	20.72
	ETR	Rand.	6.59	3.61	78.76	72.43	84.16	67.37	6.79	9.18	6.31	7.48	82.79	80.23
		FewE	5.08	2.84	73.16	66.02	84.97	67.73	57.50	39.29	56.67	37.98	40.48	56.31
		Toxin	4.23	2.10	71.84	51.18	84.14	66.92	71.14	82.22	70.31	77.85	30.22	20.72
PubMed	Retrain	Rand.	79.58	28.85	68.92	70.95	91.62	68.36	67.46	29.76	74.07	48.19	107.87	2.59
		FewE	77.73	27.99	65.14	61.47	92.30	71.30	67.46	77.19	74.08	67.20	0.02	10.61
		Toxin	53.44	13.36	74.17	63.16	90.66	70.68	85.58	88.18	78.17	69.14	18.65	12.24
	MEGU	Rand.	79.58	28.85	68.92	70.95	92.06	70.05	67.46	29.76	74.07	48.19	107.87	2.59
		FewE	77.73	27.99	65.14	61.47	92.55	71.16	67.46	77.19	74.07	67.20	0.02	10.61
		Toxin	53.44	13.36	74.17	63.16	91.17	70.42	85.58	88.18	78.17	69.14	18.65	12.24
	ETR	Rand.	79.58	28.85	68.92	70.95	91.59	69.17	67.46	29.76	74.07	48.19	107.87	2.59
		FewE	77.73	27.99	65.14	61.47	92.61	72.63	67.46	77.19	74.08	67.20	0.02	10.61
		Toxin	53.44	13.36	74.17	63.16	91.53	69.05	85.58	88.18	78.17	69.14	18.65	12.24
Photo	Retrain	Rand.	0.61	0.31	92.58	107.83	69.33	63.29	26.01	2.98	25.20	0.93	74.48	92.92
		FewE	0.61	0.31	51.46	68.21	68.03	58.10	67.44	28.76	68.02	28.74	28.12	62.26
		Toxin	0.64	0.34	44.49	52.11	66.33	49.65	86.11	85.95	85.65	80.85	13.91	30.36
	MEGU	Rand.	0.61	0.31	92.58	107.83	68.42	63.22	26.01	2.98	25.20	0.93	74.48	92.92
		FewE	0.61	0.31	51.46	68.21	68.08	57.81	67.44	28.76	68.02	28.74	28.12	62.26
		Toxin	0.64	0.34	44.49	51.83	66.36	49.06	86.11	86.27	85.65	80.66	13.91	30.43
	ETR	Rand.	0.61	0.31	92.58	107.83	68.84	63.48	26.01	2.98	25.20	0.93	74.48	92.92
		FewE	0.61	0.31	51.46	68.21	68.60	58.02	67.44	28.76	68.02	28.74	28.12	62.26
		Toxin	0.61	0.31	44.49	51.83	66.36	49.06	86.11	86.27	85.65	80.66	13.91	30.43

construction difficulty by amplifying structural ambiguity and semantic misalignment. While moderate neighborhood expansion can yield more informative signals for recovery, these signals may be distorted by over-smoothing or losing crucial semantic and structural details during information propagation, particularly within heterogeneous neighborhoods.

4.3.2 Unlearned Graph Size

Figure 3 shows that *the attack performance is unstable when the unlearned graph is small. As the graph size increases, the performance stabilizes and gradually converges across different GNN backbones*. We provide the visualization of rest metrics and corresponding analysis in Appendix B.5.

4.3.3 Node Homophily

As illustrated in Figure 3, *GraphToxin demonstrates stable performance under varying homophily levels*, with the GCN backbone achieving the strongest performance across most metrics. When node homophily approaches one, GraphSAGE and SGC diverge from GCN mainly in performance-level evaluation. Outside this extreme range, the attack performance across all backbones tends to converge. One possible explanation is that near-perfect homophilic neighborhoods produce indistinguishable node embeddings, thus leading to noninfor-

mative gradients for recovery. Similarly, the visualization and analysis of rest metrics are presented in Appendix B.6.

4.3.4 Fisher Coefficient

We evaluate the contribution of the curvature matching module by varying its Fisher coefficient (α_1) from $\{0, 0.01, 0.1, 1, 10\}$, where $\alpha_1 = 0$ serves as the ablation. Figure 4 empirically confirms the effectiveness of curvature matching, as the attack performance generally improves when the coefficient is non-zero. Consistent with previous findings, the results under worst-case removal typically exceed those under random removal. Additionally, the random case achieves higher attack fidelity when $\alpha_1 \in \{0.01, 0.1\}$ and lower posterior Wasserstein distance when $\alpha_1 \in \{0, 0.01, 0.1\}$. Overall, GraphToxin attains competitive performance when $\alpha_1 \in \{0.01, 0.1, 1\}$ and yields better results for both random and worst cases when $\alpha_1 = 0.1$.

4.3.5 Laplacian Coefficient

Figure 5 demonstrates the effectiveness of the feature smoothing module. Similar to prior studies that set Laplacian coefficients (α_2) to fairly small values [34, 50], we tune $\alpha_2 \in \{0, 1e-7, 1e-5, 1e-3, 0.1\}$. We observe that the attack performance under the worst-case removal exceeds that under

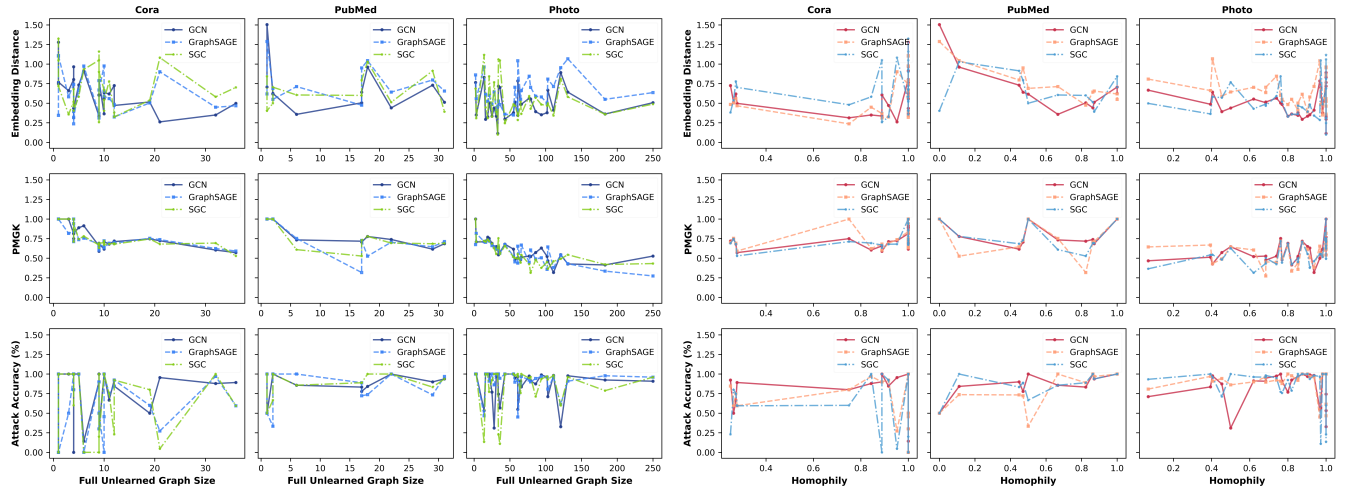


Figure 3: Impact of the Full Unlearned Graph Size and Node Homophily

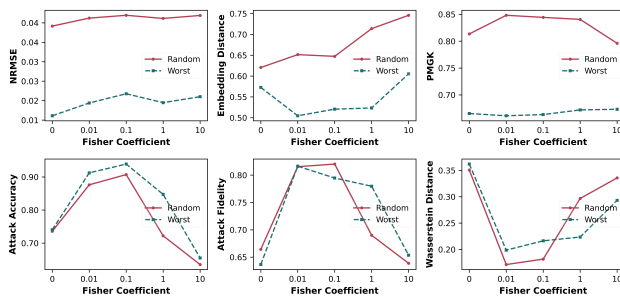


Figure 4: Impact of Fisher Coefficient

the random removal in nearly all metrics while the random case achieves stronger performance mainly in global and performance-level metrics. Overall, GraphToxin achieves superior performance when $\alpha_2 \in \{1e-7, 1e-5\}$.

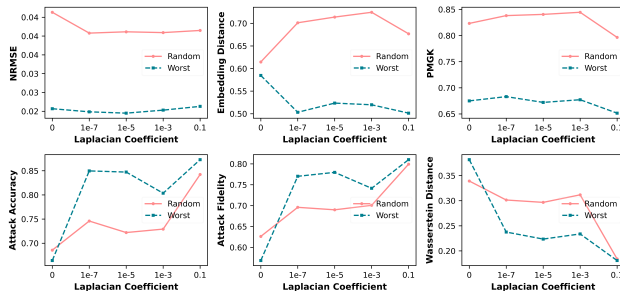


Figure 5: Impact of Laplacian Coefficient

4.4 Extensions (SQ6 and SQ7)

Due to space limitations, we provide detailed performance and analysis of the extensions to multiple-node removal and the black-box setting in Appendix B.7 and B.8, respectively.

4.5 Discussion

4.5.1 Defense (SQ8)

To investigate the performance of defense mechanisms against GraphToxin, we use the most vulnerable and stable attack target—Retraining after single-node removal in the white-box setting. We adopt both in-processing and post-processing privacy-preserving techniques. Pre-processing techniques are out of our scope as they typically alter graphs before training, making it difficult to disentangle whether observed effects stem from unlearning or from data modification.

Node-level Differential Privacy (Node-DP) in GNNs Node-DP in GNNs aims to protect an individual node and all its incident edges during message passing. Compared to standard or edge-DP, enforcing node-DP is substantially more challenging due to structural coupling and multi-hop dependencies, which amplify per-sample sensitivity and complicate privacy accounting. Existing studies either inject noises to shallow GNNs [6] or redesign architectures to decouple graph convolutions [31, 47]. Despite these efforts, achieving strong node-level privacy guarantees with competitive utility remains an open problem [19, 35, 42].

Following Xiang et al. [42], we adopt HeterPoison to implement node-DP. As the default configuration leads to severe utility degradation on GNN backbones, we directly tune the noise scale $\sigma \in \{0.006, 0.007, 0.008, 0.009, 0.01\}$ from the symmetric multivariate Laplace noise $\mathcal{LAP}(0, \sigma^2 \mathbb{I}^d)$, resulting in test accuracies of 79.40%, 76.00%, 69.90%, 61.00%

and 51.90%, respectively. We select $\sigma = 0.007$ to balance between privacy and utility.

From Table 3, *node-DP fails to effectively mitigate GraphToxin*. The reconstruction quality remains comparable to the undefended setting, and attack accuracy may even increase. We attribute this behavior to the injected DP noise, which suppresses weak and unstable gradient components while preserving more informative signals for recovery. In this sense, node-DP can act as a form of regularization, preventing GraphToxin from overfitting to trivial details.

Gradient Compression (GC). Given that GraphToxin exploits the real or surrogate gradient difference for recovery, it is imperative to enhance the privacy of released gradients. Gradient compression techniques are widely adopted against such gradient-based attacks [48]. Following Vogels et al. [37], we prune a proportion p of smaller gradients to assess the impact of gradient sparsity on GraphToxin. We experiment with high pruning ratios of $p \in \{0.5, 0.7, 0.9\}$. The most stringent case, $p = 0.9$, enforces the extreme gradient sparsity where only very few gradients are preserved. The results are shown in Table 3. Similar to node-DP, *GC cannot effectively defend GraphToxin. Preserving only partial gradients can lead to attack performance comparable to or even exceeding that obtained from full gradients. Even under extreme sparsification, GraphToxin remains competitive relative to the undefended baseline*. This finding further supports our previous speculation that retaining only important and informative gradients rather than replicating trivial details can enhance the attack performance of GraphToxin.

4.5.2 Limitation and Future Work

Assumption Relaxation Consistent with prior work [15, 34], we assume that the attacker has access to node labels and the size of the unlearned subgraph. While this assumption is standard and feasible, removing it would further enhance the applicability of GU-FGRA. One possible direction is to incorporate label inference into the GU-FGRA pipeline. When the size of the full unlearned graph is unknown, a Frobenious norm regularizer [34, 50] can be introduced to ensure graph sparsity. Furthermore, graph condensation metrics can be utilized to evaluate reconstruction quality as the ground-truth unlearned graph can be treated as an approximate condensed target. We leave these extensions for future work.

Large-scale Node Removal This work follows existing graph unlearning research and primarily examines the effectiveness of GraphToxin under relatively small-scale node removal. Although we explore the challenging worst-case scenarios that generate comparatively larger unlearned graphs by simultaneously removing multiple highest-degree nodes, investigating the scalability of GraphToxin under large-scale multiple-node removal presents a promising direction for future work.

Beyond Degree-Based Worst-case Analysis Node degree provides a direct and interpretable proxy for structural influ-

ence in the worst-case evaluation, as deleting a node necessarily removes all of its incident edges. This correspondence makes degree a natural criterion for modeling the immediate structural impact of unlearning requests, while other measures such as node influence [20, 41], may capture different worst-case behaviors. Exploring alternative influence criteria could provide a more comprehensive view of GU-FGRA.

Deep Investigation on Complex Interactions Several non-trivial findings emerge from the experimental results. For instance, GraphToxin remains effective under strict differential privacy guarantees, and retaining only a small fraction of gradients can suffice for GU-FGRA. These observations suggest complex interactions among model architectures, graph sparsity, node homophily and other possible factors. A deeper investigation on these factors is left for future work.

5 Related Work

5.1 Graph Unlearning

Existing graph unlearning methods are commonly categorized into exact unlearning and approximate unlearning [30].

5.1.1 Exact Graph Unlearning

GraphEraser pioneered the first graph unlearning framework [3]. This framework partitions the original training graph into disjoint shards and trains a separate GNN on each shard. Upon receiving a new unlearning request, the target node is removed from its associated shard, followed by retraining of the corresponding shard model. Wang et al. [38] subsequently extended this framework to inductive settings.

5.1.2 Approximate Graph Unlearning

GIF [41] utilizes graph influence functions to estimate parameter changes induced by node deletion and subsequently applies corrective updates to model parameters to approximate the state of a model retrained on the remaining graph. GNNDelete [28] formulates unlearning as an optimization problem with two objectives: deleted edge consistency, which removes the influence of deleted edges from model parameters and neighboring representations, and neighborhood influence preservation, which ensures that retained model knowledge is unaffected after deletion. MEGU [21] introduces a mutual evolution framework that jointly optimizes a predictive module and an unlearning module to generate effective and reliable unlearning performance. ETR [43] proposes a training-free two-stage unlearning framework. In the Erase stage, ETR modifies model parameters to mitigate the impact of deleted nodes and their propagated influence on neighboring nodes. while the Rectify stage approximates the gradients of the remaining nodes to enhance utility after graph unlearning.

Table 3: The Performance of Node-DP and Gradient Compression in Defending GraphToxin (Dataset: Cora). Unit: **1e-2**. Arrow indicates the direction of better performance and the **bold** font denotes the ‘best’ results.

Defense	Type	RNMSE(\downarrow)		ED(\downarrow)		PMGK(\uparrow)		ACC(\uparrow)		FID(\uparrow)		PWD(\downarrow)	
		Random	Worst	Random	Worst	Random	Worst	Random	Worst	Random	Worst	Random	Worst
DP	Node	5.88	3.02	67.95	61.79	82.39	65.44	86.72	89.87	57.06	73.69	44.84	45.15
GC	p-0.5	4.15	2.05	70.40	48.40	83.81	67.20	76.62	92.81	68.64	79.26	31.21	17.50
	p-0.7	4.29	2.15	70.06	50.99	83.27	66.16	73.28	86.60	71.50	80.54	26.74	18.44
	p-0.9	4.14	2.15	66.35	46.17	82.53	67.27	79.53	90.31	74.17	79.60	24.24	17.79

5.2 Graph Reconstruction Attacks

Existing graph reconstruction attacks against GNNs can be broadly categorized into four groups based on their attack objectives and assumptions.

5.2.1 Link Stealing Attack

Link stealing attacks aim to infer the existence of edges in a target graph. He et al. [13] introduced the first link stealing attack and provided a comprehensive attack taxonomy using various background knowledge. LinkTeller [39] exploits node features and labels to propose the first query-based link stealing attack via influence analysis in both transductive and inductive settings. LinkThief [49] combines node similarity, generalized structural features, and shadow graphs to assist link membership inference. Recently, TrendAttack [46] emerged as the first link stealing attack against graph unlearning to identify the link membership through confidence trends. This line of work focuses on edge-level removal, however, node removal introduces substantially broader structural changes and poses greater reconstruction challenges.

5.2.2 Attribute Inference Attack against GNNs

Attribute inference attacks seek to recover sensitive attributes rather than graph structure. Duddu et al. [8] proposed the first attribute inference attack against GNNs. They exploited node embeddings of partial nodes and their associated sensitive features to train a supervised attack classifier for inferring sensitive attributes of the target nodes. Olatunji et al. [27] developed three attribute inference attacks that leverage partial sensitive attributes, public non-sensitive attributes and shadow graphs to conduct multiple queries. These attacks solely target sensitive attributes, rather than full node feature recovery, which is a central focus of our work.

5.2.3 Graph Topology Reconstruction Attack

Graph topology reconstruction attacks aim to recover the adjacency structure of the target graph. Duddu et al. [8] designed the first graph topology reconstruction attack to exploit a strong correlation between publicly released embeddings and the ground-truth graph topology. Building on the same attack setting, GraphMI [51] and Zhang et al. [52] reconstructed

graph topology with graph statistics similar to the ground-truth through a graph encoder-decoder architectures. Olatunji et al. [26] employed node features and their explanations to guide topology recovery by jointly minimizing reconstruction errors on node features and explanations and prediction losses. These methods reconstruct only graph topology and depend on assumptions that require feature or explanation access, thereby restricting their applicability and failing to generalize to fully data-free black-box settings.

5.2.4 Gradient Inversion Attack

While the above three attack types have broad application scenarios, gradient inversion attacks against GNNs are specifically tailored for graph federated learning. GRAIN [7] presents the first gradient inversion attack for partial node feature and graph topology recovery. It initially exploits rank deficiencies in GNN layers to reconstruct candidate subgraphs, then iteratively filters unreliable ones, and finally combines these candidates with a depth-first search strategy for graph recovery. GLG [34] demonstrates that gradient matching enables recovery of subgraphs in both node and graph-level tasks. However, these attacks assume access to client-side gradients and cannot be trivially adapted to graph unlearning.

6 Conclusion

In this study, we pioneer the investigation into the vulnerabilities of reconstructing the full unlearned graphs through graph unlearning. We propose GraphToxin, the first full graph reconstruction attack against graph unlearning. Specifically, we introduce a novel curvature matching module to provide fine-grained signals for full unlearned graph recovery. We further extend GraphToxin to multiple-node removal under both white-box and black-box settings. Furthermore, we present a comprehensive evaluation framework, demonstrating the necessity of worst-case evaluation and multi-level evaluation metrics. Extensive experiments demonstrates the effectiveness and flexibility of GraphToxin across both white-box and black-box settings for single and multiple-node removal. In addition, our assessment of existing defense mechanisms shows that they provide limited protection and may exhibit unintended effects against this attack, highlighting the urgent need to develop more robust defenses for graph unlearning.

APPENDIX

Ethical Considerations

This study investigates vulnerabilities of graph unlearning solely on publicly available benchmark datasets and with unlearning algorithms tested on local devices. It does not directly compromise personal information or cause harm to real-world systems or servers. As a red team, we validate that the proposed attack reveals substantially more sensitive information than existing inference attacks. The findings underscore the urgent need for robust countermeasures.

Open Science

In accordance with the CFP’s Open Science guidelines, we release the artifacts required to reproduce our experiments, including the datasets, code, implementation details, and evaluation pipeline. To preserve anonymity during review, these materials are hosted in an anonymous repository <https://anonymous.4open.science/r/GraphToxin-A854>, and will be migrated to a public GitHub repository upon acceptance. This artifact release is intended to facilitate further investigation into vulnerabilities in graph unlearning and to inspire future work on robust defenses.

A Theorem Assumptions and Proof

The subsequent theoretical proof of curvature matching is built upon the following two assumptions:

Assumption 1 (Empirical Risk Function). *We assume that $\mathcal{L}(\cdot)$ is twice continuously differentiable and the Hessian $H = \nabla^2 \mathcal{L}(\theta)$ is invertible and symmetric w.r.t. parameter θ . Following previous studies [4, 45], we add a damping term λI to H if $\mathcal{L}(\cdot)$ is non-convex.*

Assumption 2 (Small Parameter Change). *We assume that the parameter change $\theta^* - \theta$ before and after graph unlearning is small.*

We empirically observe that this change is small, as reflected in our experimental results. This observation is consistent with the objective of graph unlearning and is theoretically bounded in prior work [5, 41].

Under the above assumptions, the first-order Taylor expansion of the gradient $\nabla \mathcal{L}(\cdot)$ around a stationary point θ is:

$$\nabla \mathcal{L}(\theta^*) \approx \nabla \mathcal{L}(\theta) + \nabla^2 \mathcal{L}(\theta)(\theta^* - \theta) \quad (14)$$

Gradient-based GU-FGRA initializes a dummy graph and iteratively optimizes it to recover a final graph whose induced gradients explain the observed parameter changes [15]. Hence:

$$\Delta \tilde{\nabla} \approx \theta^* - \theta \quad (15)$$

where $\Delta \tilde{\nabla}$ denotes the parameter change induced by the dummy graph. Since the original model is already trained and released, its parameters θ are fixed. Without loss of generality, GU-FGRA aims to recover parameters $\tilde{\theta}$ such that $\Delta \tilde{\nabla} = \tilde{\theta} - \theta$.

Based on Equation (14) and Equation (15), we provide the proof of Theorem 1 below:

Proof. Based on Equation (14), we get $\Delta \nabla \approx H(\theta^* - \theta)$. Since H is invertible, $\theta^* - \theta \approx H^{-1} \Delta \nabla$. As for Equation (15), $\tilde{\theta} - \theta \approx H^{-1} \Delta \tilde{\nabla}$. Therefore, the attack goal is transformed to minimize the difference between $H^{-1} \Delta \nabla$ and $H^{-1} \Delta \tilde{\nabla}$. Formally, $H^{-1}(\Delta \tilde{\nabla} - \Delta \nabla) \approx 0$. Take the $H^{1/2}$ to the left-hand and right-hand side, then we get $H^{-1/2}(\Delta \tilde{\nabla} - \Delta \nabla) \approx 0$. Consider the squared L2 norm, the previous approximation equals to $(\Delta \tilde{\nabla} - \Delta \nabla)^T H^{-1}(\Delta \tilde{\nabla} - \Delta \nabla)$, hereby completing the proof.

B Experimental Validation

B.1 Datasets

Cora and PubMed are small-scale and medium-scale citation networks with low average node degrees, where nodes represent scientific/medical publications, edges denote citations, and node features carry author’s personal information. Photo is a dense co-purchase graph, where nodes represent products, edges indicate frequent co-purchases, and features encode product reviews. The dataset statistics are shown in Table 4. We follow the standard data split setting commonly used in GNN benchmarks [28, 32], randomly selecting 20 nodes per class for training, 30 nodes per class for validation, and using the remaining nodes for testing.

Table 4: Detailed Graph Statistics

Datasets	Nodes	Edges	Features	Labels	Avg. Deg.	Homo. (%)
Cora	2,708	10,556	1,433	7	3.90	82.52
PubMed	19,717	88,648	500	3	4.50	79.24
Photo	7,650	238,162	745	8	31.13	83.65

B.2 Implementation

- Victim GNN:** We consider 2-layer GNNs with the hidden dimension of 256 and a linear classifier for node classification tasks. We tune the learning rate from $\{0.001, 0.005\}$, and set the weight decay as $5e-4$ and training epochs as 200.
- Graph Unlearning:** For MEGU, we adopt the default setting to set the unlearning rate as 0.05, weight decay as $1e-4$, tuning epoch as 100, and coefficients in the propagation process as 0.8, 0.5 and the coefficient in the loss function as 0.01. For ETR, we follow their default setting to tune the parameter-rectifying coefficient λ from $\{0.001, 0.01, 0.3\}$.

3. **GraphToxin**: For single-node removal, we randomly sample 10% of training nodes or select the top 10% highest-degree nodes as attack targets, and report their average results throughout our paper. The attacker does not have access to the locations of the removed nodes and only observes the gradient difference between the original and the unlearned GNNs. Unless otherwise specified, the Fisher coefficient is set to 1 and the Laplacian coefficient is set to $1e-5$. AdamW [23] is used as the optimizer. Since multiple restarts to the optimizer (e.g., L-BFGS) from different starting points can significantly improve the reconstruction quality, for a fair comparison, we strictly follow the configuration in Sinha et.al. [34] for all experiments and only report the attack results with a single run of the optimizer. In addition, we strictly set the attack learning rate as 0.01 for all experiments. Following Geiping et al. [11] and Hu et al. [15], each optimization is run for up to 10,000 iterations, with most attacks converging earlier, and a step size decay is applied after $3/8$, $5/8$, $7/8$ of total iterations, using the multiplicative factor of 0.5.

B.3 Original and Unlearning Performance

Table 5 shows that all graph unlearning methods exhibit comparable performance across the three GNN backbones, with variations within 1%. As for GNN backbones, the GCN backbone achieves the highest performance on Cora and PubMed while SGC performs best on Photo, with differences of less than 2% compared to GCN. Across unlearning methods, ETR preserves model utility more effectively on Cora and PubMed, while Retraining exceeds other unlearning methods with GCN and SGC backbones. In contrast, MEGU yields the strongest results with GraphSAGE on Photo. Regarding removal settings, removing the 10% of the highest-degree nodes results in larger benign performance degradation compared to the random-node removal, which is amplified on sparse and smaller-scale graphs.

B.4 Attack with GNN Backbones

As shown in Table 6, *GraphToxin consistently retains its superiority and generalization across all GNN backbones and graph datasets*. Taken together, these results suggest that there is no universally most vulnerable GNN due to the complex interactions among model architecture, graph sparsity and homophily. We provide the following plausible explanations: (1) GCN aggregates information over local neighborhoods, which makes node representations strongly dependent on features propagated from their local neighborhoods. This propagation can provide more informative gradient signals for recovering underlying graph structure. However, on dense graphs, rapid neighborhood expansion can lead to over-smoothing, weakening node-specific signals. As a result, GCN tends to

achieve more competitive performance on small-scale and sparse graphs such as Cora. (2) GraphSAGE relies on random neighbor sampling rather than full neighborhood aggregation. Consequently, gradients are computed from incomplete and randomly varying local structures, which might obfuscate the gradient-based guidance for recovery, particularly on sparse graphs. While on dense graphs such as Photo, structural redundancy can offset the randomness introduced by neighbor sampling, enabling GraphToxin with the GraphSAGE backbone to maintain strong reconstruction performance. (3) SGC employs linear multi-hop feature propagation. Although its linearity offers a more direct and simpler proxy for full graph recovery, it can suppress fine-grained and node-specific details. This dual effect might explain why SGC performs well in some metrics on PubMed and Photo, yet exhibits degraded performance on Cora.

B.5 Impact Factor - Unlearned Graph Size

From Figures 3 and 6, RNMSE remains consistently low with minimal variation, indicating its insensitivity to the unlearned graph size. PMGK generally decreases as the graph size increases. An exception is observed on Photo with the GCN backbone, where PMGK rebounds when the deletion graph becomes sufficiently large. ED and PWD also exhibit a decreasing trend with increasing unlearned graph size. In addition, attack accuracy and fidelity show noticeable oscillations. These variations arise from single-node removal, where each target node induces an unlearned graph of different sizes and structural complexity. The results are then sorted by the size of the unlearned graph. Heterogeneity across target nodes leads to varying reconstruction difficulty, which manifests as fluctuations in the plotted results.

B.6 Impact Factor - Node Homophily

Consistent with the analysis on unlearned graph size, RNMSE remains largely invariant to changes in the homophily of unlearned nodes. However, other metrics exhibit clearer correlations with node homophily: PMGK as well as attack accuracy and fidelity are positively correlated with homophily, whereas ED and PWD are negatively correlated. Overall, these observations *indicate that node homophily may serve as a more informative indicator than unlearned graph size for characterizing the vulnerability of GU-FGRA*. We leave the deeper investigation for future work.

B.7 Multiple Node Removal

In this section, we examine the effectiveness of GraphToxin under multiple-node removal, where 5, 10, and 15 nodes are simultaneously removed from the training graph, respectively. For a fair comparison, all hyperparameters are kept identical to those in single-node removal. Under the random removal

Table 5: The Performance of the Original and Unlearned GNNs for A Single Node Removal

Dataset	GNN	Original		Retraining				MEGU				ETR			
		Random		Worst		Random		Worst		Random		Worst			
		ACC	AUC												
Cora	GCN	80.20	96.70	80.05	96.68	79.99	96.67	80.06	96.66	80.52	96.69	80.57	96.76	80.69	96.77
	SAGE	81.10	96.61	80.99	96.66	80.77	96.64	80.04	96.54	79.94	96.52	80.80	96.56	80.86	96.57
	SGC	81.10	96.12	80.42	96.24	80.24	96.19	80.64	96.06	80.49	96.06	81.10	96.15	81.10	96.17
PubMed	GCN	77.40	90.44	77.78	90.53	77.93	90.40	77.12	90.28	76.68	90.32	77.53	90.45	77.75	90.46
	SAGE	76.90	89.44	75.53	89.23	74.80	89.08	76.22	89.51	76.05	89.50	76.68	89.54	76.48	89.53
	SGC	78.20	90.37	77.92	90.44	77.78	90.29	75.25	89.65	75.72	90.03	78.05	89.90	78.12	89.95
Photo	GCN	90.07	99.06	91.09	99.05	91.03	99.06	89.11	98.90	89.47	98.96	88.19	98.71	88.26	98.72
	SAGE	91.31	99.28	89.22	99.05	89.86	99.09	90.40	99.14	90.15	99.14	80.45	93.14	80.38	93.13
	SGC	92.04	99.02	91.14	98.99	91.40	99.00	91.08	98.88	90.97	98.94	90.11	99.03	90.12	99.03

 Table 6: GraphToxin for A Single Node Removal with Different GNN Backbones (GU: Retraining). Unit: 1e-2. Arrow indicates the direction of better performance and the blue color denotes the superb ‘best’ results (in **bold**).

Dataset	GNN	Baseline	NRMSE(\downarrow)		ED(\downarrow)		PMGK(\uparrow)		ATT. ACC(\uparrow)		ATT. FID(\uparrow)		PWD(\downarrow)	
			Random	Worst	Random	Worst	Random	Worst	Random	Worst	Random	Worst	Random	Worst
Cora	GCN	Rand.	6.59	3.61	78.76	72.45	84.35	68.35	6.79	9.18	6.31	7.48	82.79	80.23
		FewE	5.08	2.84	73.11	65.96	84.62	68.79	57.50	39.29	56.67	37.98	40.47	56.30
		Toxin	4.11	1.95	71.38	52.35	84.05	67.21	72.21	84.72	69.00	77.97	29.66	22.35
	SAGE	Rand.	6.59	3.61	65.84	63.10	81.13	66.78	6.79	9.18	5.60	6.66	89.97	91.17
		FewE	6.01	3.24	67.71	64.14	80.10	66.94	38.69	28.63	33.93	24.36	56.19	65.42
		Toxin	4.49	1.86	60.20	57.46	82.02	67.10	68.21	64.36	62.26	55.17	33.93	38.72
	SGC	Rand.	6.59	3.61	95.25	91.71	81.41	67.04	6.79	9.18	8.10	9.26	84.98	80.48
		FewE	6.02	3.38	79.64	80.47	80.32	67.60	32.14	28.66	32.86	28.76	63.28	68.44
		Toxin	4.35	2.16	65.47	66.94	84.04	67.56	72.50	61.03	67.50	55.99	30.97	41.89
PubMed	GCN	Rand.	79.58	28.85	68.92	70.95	91.62	68.36	67.46	29.76	74.07	48.19	107.87	2.59
		FewE	77.73	27.99	65.14	61.47	92.30	71.30	67.46	77.19	74.08	67.20	0.02	10.61
		Toxin	53.44	13.36	74.17	63.16	90.66	70.68	85.58	88.18	78.17	69.14	18.65	12.24
	SAGE	Rand.	79.58	28.85	125.38	99.69	91.28	72.51	16.80	27.29	1.85	33.33	59.51	50.23
		FewE	79.12	28.03	86.45	74.73	93.24	69.55	65.21	64.13	55.82	64.16	25.55	32.54
		Toxin	56.36	8.64	80.12	76.06	91.32	60.54	75.93	84.17	66.53	73.65	26.97	21.28
	SGC	Rand.	79.58	28.85	81.82	83.96	91.55	69.86	67.46	29.76	73.15	46.39	0.00	2.90
		FewE	78.89	28.79	67.72	88.19	91.99	69.92	63.10	70.08	58.33	53.30	22.43	19.82
		Toxin	42.97	14.55	64.16	70.67	88.98	68.42	81.88	92.48	81.88	69.40	2.01	12.28
Photo	GCN	Rand.	0.61	0.31	92.58	107.83	69.33	63.29	26.01	2.98	25.20	0.93	74.48	92.92
		FewE	0.61	0.31	51.46	68.21	68.03	58.10	67.44	28.76	68.02	28.74	28.12	62.26
		Toxin	0.64	0.34	44.49	52.11	66.33	49.65	86.11	85.95	85.65	80.85	13.91	30.36
	SAGE	Rand.	0.61	0.31	116.19	127.18	70.49	65.60	26.01	2.98	26.56	3.89	74.77	95.12
		FewE	0.62	0.33	72.00	100.15	65.23	56.95	65.29	29.26	66.60	29.32	29.88	64.59
		Toxin	0.65	0.34	55.44	70.72	62.42	48.22	94.52	87.79	91.74	81.67	11.51	30.41
	SGC	Rand.	0.61	0.31	94.57	111.16	71.23	63.74	26.01	2.98	25.20	1.25	74.11	92.11
		FewE	0.61	0.31	58.26	56.17	68.42	60.97	64.69	45.54	65.99	47.94	26.50	41.42
		Toxin	0.66	0.33	56.02	47.60	65.29	45.59	80.78	90.39	76.55	85.76	21.05	26.89

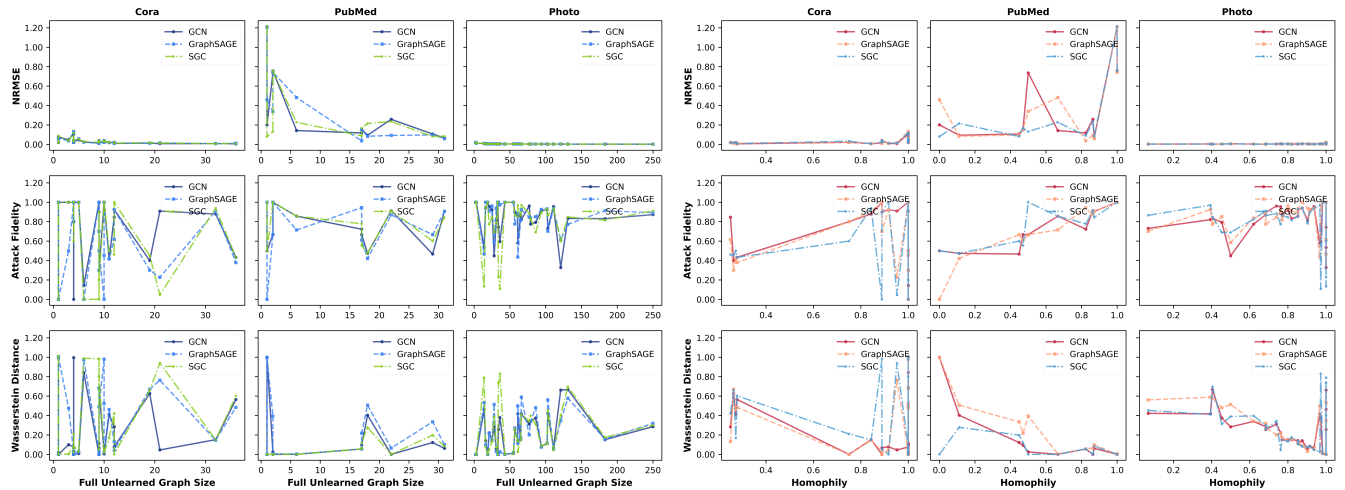


Figure 6: Impact of the Full Unlearned Graph Size and Node Homophily

setting, we sample 5 disjoint node sets with the same removal size, while in the worst-case removal setting, we select the top 25, 50, 75 highest-degree nodes and partition them into five non-overlapping sets based on their degree ranking. The average results are reported in Table 7.

Under the worst-case multiple-node removal, the unlearning performance of Retraining improves in accuracy but slightly decline in AUC when more nodes are removed. In terms of attack performance, GraphToxin consistently outperforms other baselines. As the number of removed nodes increases, reconstruction-related metrics generally yield better results. In contrast, performance-level metrics display a non-monotonic pattern, which initially increase and then slightly degrade. Additionally, the random-case and worst-case scenarios exhibit complementary strengths, with neither consistently dominating the other across all metrics. This observation *highlights the necessity of considering both scenarios for a comprehensive evaluation*.

B.8 Black-box Setting

Setup We now assess the performance of GraphToxin under a data-free, black-box setting. Following the configuration in Zhuang et al. [54], we utilize a GCN with 2 layers and 256 hidden units as a surrogate model, and a 3-layer MLP with 128 and 256 hidden units as a full-parameter graph generator. We set the query graph size as 250 with 32 feature dimensions. During model stealing, each query encompasses training the generator 2 times with a learning rate of $1e-6$ and training the surrogate 5 times with a learning rate of 0.001. The total number of queries is set to 100. The stealing performance of the original GNN is 79.40% in accuracy and 96.12% in AUC. After unlearning, the stealing performance of the unlearned GNN under both single and multiple-node removal improves

in accuracy while slightly declines in AUC. As for GU-FGRA, we adopt the same hyperparameter settings as in the white-box experiments. For the semantic calibration module, we set its coefficient as 50 for single-node removal and 5000 for multiple-node removal, as the latter introduces substantially higher noise. Average results are reported in Table 8.

Single Node Removal We observe that *black-box GraphToxin consistently outperforms all baselines under single-node removal*. Since we introduce the semantic calibration module to enforce the label alignment, the overall attack performance in the performance-level metrics is competitive, although the performance in reconstruction-related metrics degrades relative to the white-box setting as expected. A plausible explanation is that black-box GraphToxin utilizes the semantic calibration during recovery, which might shift some nodes across the model’s decision boundary to obtain the correct predictions but ignore the actual distance in feature or embedding space. Overall, the degradation in such metrics remains acceptable.

Multiple Node Removal *Under the black-box multi-node removal setting, GraphToxin still exceeds other baselines*. Compared to single-node removal, performance-level metrics decline when more nodes are unlearned. However, the attack results of the reconstruction-related metrics are mixed. PMGK and ED decrease, while NRMSE improves in both random and worst-case node removal scenarios.

Table 7: **GraphToxin for Multiple Node Removals Based on Retraining (Backbone: GCN, Dataset: Cora)**. Unit: **1e-2**. Arrow indicates the direction of better performance and the **blue** color denotes the superb ‘best’ results (in **bold**).

Rem. Num	Retraining(ACC/AUC)		Baseline	NRMSE(↓)		ED(↓)		PMGK(↑)		ACC(↑)		FID(↑)		PWD(↓)	
	Random	Worst		Random	Worst	Random	Worst	Random	Worst	Random	Worst	Random	Worst	Random	Worst
5	80.22/96.64	80.30/96.66	Rand. FewE Toxin	2.34	1.71	73.16	73.52	68.01	62.14	27.88	9.94	23.80	8.68	67.08	77.68
				2.13	1.65	61.95	62.41	70.47	60.59	28.75	20.02	28.78	20.15	66.79	72.13
				1.66	1.03	56.27	54.59	70.45	64.82	60.03	70.40	52.06	63.98	47.24	39.08
10	79.98/96.50	80.44/96.49	Rand. FewE Toxin	1.69	1.42	72.50	73.56	58.88	63.76	24.84	17.72	22.04	16.00	66.75	72.57
				1.58	1.31	60.10	59.51	64.65	68.37	24.80	20.54	23.63	17.99	65.72	68.30
				0.99	0.73	54.36	52.29	65.78	68.64	67.83	64.47	59.12	58.99	39.79	44.09
15	79.46/96.57	79.84/96.47	Rand. FewE Toxin	1.41	1.28	73.37	74.06	63.11	62.27	21.28	16.61	19.87	15.21	70.53	75.92
				1.32	1.18	57.73	58.69	70.05	69.47	22.71	17.38	21.82	16.31	67.23	72.32
				0.80	0.69	54.06	55.67	66.05	70.34	65.63	58.79	53.80	53.50	51.01	51.05

Table 8: **Black-box GraphToxin for A Single and Multiple Node Removals Based on Retraining (Dataset: Cora)**. Unit: **1e-2**. Arrow indicates the direction of better performance and the **blue** color denotes the superb ‘best’ results (in **bold**).

Type	Retraining(ACC/AUC)		Baseline	NRMSE(↓)		ED(↓)		PMGK(↑)		ACC(↑)		FID(↑)		PWD(↓)	
	Random	Worst		Random	Worst	Random	Worst	Random	Worst	Random	Worst	Random	Worst	Random	Worst
Single	79.66/96.10	79.63/96.09	Rand. FewE Toxin	11.51	6.29	127.87	120.86	81.09	67.11	12.20	13.85	13.51	14.40	16.19	14.64
				5.68	3.10	115.91	96.78	82.98	67.97	49.40	65.56	47.62	58.30	11.27	9.25
				4.76	2.49	87.37	80.08	81.56	68.30	72.74	82.07	70.95	73.64	8.28	6.97
Multiple	79.86/96.09	79.78/96.10	Rand. FewE Toxin	2.34	1.71	126.49	135.71	65.10	57.04	27.88	9.94	21.81	7.57	14.91	17.83
				2.35	1.72	111.55	114.68	69.47	59.83	41.92	38.55	33.20	33.63	13.22	12.76
				1.53	1.07	90.04	71.66	67.70	59.93	59.41	69.60	47.88	60.11	11.56	9.63

References

- [1] Martin Andres Bertran, Shuai Tang, Michael Kearns, Jamie Heather Morgenstern, Aaron Roth, and Steven Wu. Reconstruction attacks on machine unlearning: Simple models are vulnerable. In *The Thirty-eighth Annual Conference on Neural Information Processing Systems*, 2024.
- [2] Min Chen, Zhikun Zhang, Tianhao Wang, Michael Backes, Mathias Humbert, and Yang Zhang. When machine unlearning jeopardizes privacy. In *Proceedings of the 2021 ACM SIGSAC Conference on Computer and Communications Security*, CCS '21, page 896–911, New York, NY, USA, 2021. Association for Computing Machinery.
- [3] Min Chen, Zhikun Zhang, Tianhao Wang, Michael Backes, Mathias Humbert, and Yang Zhang. Graph unlearning. In *Proceedings of the 2022 ACM SIGSAC Conference on Computer and Communications Security*, CCS '22, page 499–513, New York, NY, USA, 2022. Association for Computing Machinery.
- [4] Zizhang Chen, Peizhao Li, Hongfu Liu, and Pengyu Hong. Characterizing the influence of graph elements. In *The Eleventh International Conference on Learning Representations*, 2023.
- [5] Eli Chien, Chao Pan, and Olgica Milenkovic. Certified graph unlearning. In *NeurIPS 2022 Workshop: New Frontiers in Graph Learning*, 2022.
- [6] Ameya Daigavane, Gagan Madan, Aditya Sinha, Abhradeep Guha Thakurta, Gaurav Aggarwal, and Prateek Jain. Node-level differentially private graph neural networks, 2022.
- [7] Maria Drencheva, Ivo Petrov, Maximilian Baader, Dimitar Iliev Dimitrov, and Martin Vechev. GRAIN: Exact graph reconstruction from gradients. In *The Thirteenth International Conference on Learning Representations*, 2025.
- [8] Vasisht Duddu, Antoine Boutet, and Virat Shejwalkar. Quantifying privacy leakage in graph embedding. In *MobiQuitous 2020 - 17th EAI International Conference on Mobile and Ubiquitous Systems: Computing, Networking and Services*, MobiQuitous '20, page 76–85, New York, NY, USA, 2021. Association for Computing Machinery.
- [9] Mingyuan Fan, Fuyi Wang, Cen Chen, and Jianying Zhou. Boosting gradient leakage attacks: data reconstruction in realistic fl settings. In *Proceedings of the 34th USENIX Conference on Security Symposium*, SEC '25, USA, 2025. USENIX Association.
- [10] Chong Fu, Xuhong Zhang, Shouling Ji, Jinyin Chen, Jingzheng Wu, Shanqing Guo, Jun Zhou, Alex X. Liu, and Ting Wang. Label inference attacks against vertical federated learning. In *31st USENIX Security Symposium (USENIX Security 22)*, pages 1397–1414, Boston, MA, August 2022. USENIX Association.
- [11] Jonas Geiping, Hartmut Bauermeister, Hannah Dröge, and Michael Moeller. Inverting gradients - how easy is it to break privacy in federated learning? In *Proceedings of the 34th International Conference on Neural Information Processing Systems*, NIPS '20, Red Hook, NY, USA, 2020. Curran Associates Inc.
- [12] William L. Hamilton, Rex Ying, and Jure Leskovec. Inductive representation learning on large graphs. In *Proceedings of the 31st International Conference on Neural Information Processing Systems*, NIPS'17, page 1025–1035, Red Hook, NY, USA, 2017. Curran Associates Inc.
- [13] Xinlei He, Jinyuan Jia, Michael Backes, Neil Zhenqiang Gong, and Yang Zhang. Stealing links from graph neural networks. In *30th USENIX Security Symposium (USENIX Security 21)*, pages 2669–2686. USENIX Association, August 2021.
- [14] Kalle Hjerppe, Jukka Ruohonen, and Ville Leppanen. The general data protection regulation: Requirements, architectures, and constraints. In *2019 IEEE 27th International Requirements Engineering Conference (RE)*. IEEE, September 2019.

[15] Hongsheng Hu, Shuo Wang, Tian Dong, and Minhui Xue. Learn what you want to unlearn: Unlearning inversion attacks against machine unlearning. In *2024 IEEE Symposium on Security and Privacy (SP)*, pages 3257–3275, 2024.

[16] Vassilis Kalofolias. How to learn a graph from smooth signals. In Arthur Gretton and Christian C. Robert, editors, *Proceedings of the 19th International Conference on Artificial Intelligence and Statistics*, volume 51 of *Proceedings of Machine Learning Research*, pages 920–929, Cadiz, Spain, 09–11 May 2016. PMLR.

[17] Ryo Karakida, Shotaro Akaho, and Shun-ichi Amari. Universal statistics of fisher information in deep neural networks: Mean field approach. In Kamalika Chaudhuri and Masashi Sugiyama, editors, *Proceedings of the Twenty-Second International Conference on Artificial Intelligence and Statistics*, volume 89 of *Proceedings of Machine Learning Research*, pages 1032–1041. PMLR, 16–18 Apr 2019.

[18] Thomas N. Kipf and Max Welling. Semi-supervised classification with graph convolutional networks. In *International Conference on Learning Representations*, 2017.

[19] Dian Lei, Zijun Song, Yanli Yuan, Chunhai Li, and Liehuang Zhu. Achieving personalized privacy-preserving graph neural network via topology awareness. In *Proceedings of the ACM on Web Conference 2025, WWW '25*, page 3552–3560, New York, NY, USA, 2025. Association for Computing Machinery.

[20] Weikai Li, Zhiping Xiao, Xiao Luo, and Yizhou Sun. Fast inference of removal-based node influence. In *Proceedings of the ACM Web Conference 2024, WWW '24*, page 422–433, New York, NY, USA, 2024. Association for Computing Machinery.

[21] Xunkai Li, Yulin Zhao, Zhengyu Wu, Wentao Zhang, Rong-Hua Li, and Guoren Wang. Towards effective and general graph unlearning via mutual evolution. *Proceedings of the AAAI Conference on Artificial Intelligence*, 38(12):13682–13690, Mar. 2024.

[22] Can Liu, Jin Wang, , Yipeng Zhou, Yachao Yuan, Quanzheng Sheng, and Kejie Lu. Afgi: Towards accurate and fast-convergent gradient inversion attack in federated learning, 2024.

[23] Ilya Loshchilov and Frank Hutter. Decoupled weight decay regularization. In *International Conference on Learning Representations*, 2019.

[24] Haoran Lu, Lei Wang, Xiaoliang Ma, Jun Cheng, and Mengchu Zhou. A survey of graph neural networks and their industrial applications. *Neurocomputing*, 614:128761, 2025.

[25] Giannis Nikolentzos, Polykarpos Meladianos, and Michalis Vazirgiannis. Matching node embeddings for graph similarity. *Proceedings of the AAAI Conference on Artificial Intelligence*, 31(1), Feb. 2017.

[26] Iyiola Olatunji, Mandeep Rathee, Thorben Funke, and Megha Khosla. Private graph extraction via feature explanations. *Proceedings on Privacy Enhancing Technologies*, 2023:59–78, 04 2023.

[27] Iyiola E. Olatunji, Anmar Hizber, Oliver Sihlovec, and Megha Khosla. Does black-box attribute inference attacks on graph neural networks constitute privacy risk?, 2023.

[28] Yijian Qin, Ziwei Zhang, Xin Wang, Zeyang Zhang, and Wenwu Zhu. Nas-bench-graph: Benchmarking graph neural architecture search. In S. Koyejo, S. Mohamed, A. Agarwal, D. Belgrave, K. Cho, and A. Oh, editors, *Advances in Neural Information Processing Systems*, volume 35, pages 54–69. Curran Associates, Inc., 2022.

[29] Alexandre Rame, Corentin Dancette, and Matthieu Cord. Fishr: Invariant gradient variances for out-of-distribution generalization. In Kamalika Chaudhuri, Stefanie Jegelka, Le Song, Csaba Szepesvari, Gang Niu, and Sivan Sabato, editors, *Proceedings of the 39th International Conference on Machine Learning*, volume 162 of *Proceedings of Machine Learning Research*, pages 18347–18377. PMLR, 17–23 Jul 2022.

[30] Anwar Said, Yuying Zhao, Tyler Derr, Mudassir Shabbir, Waseem Abbas, and Xenofon Koutsoukos. A survey of graph unlearning, 2024.

[31] Sina Sajadmanesh, Ali Shahin Shamsabadi, Aurélien Bellet, and Daniel Gatica-Perez. Gap: Differentially private graph neural networks with aggregation perturbation. In *32nd USENIX Security Symposium (USENIX Security 23)*, Anaheim, CA, August 2023. USENIX Association.

[32] Oleksandr Shchur, Maximilian Mumme, Aleksandar Bojchevski, and Stephan Günnemann. Pitfalls of graph neural network evaluation. *ArXiv*, abs/1811.05868, 2018.

[33] Giannis Siglidis, Giannis Nikolentzos, Stratis Limnios, Christos Giatsidis, Konstantinos Skianis, and Michalis Vazirgiannis. Grakel: A graph kernel library in python. *Journal of Machine Learning Research*, 21(54):1–5, 2020.

[34] Divya Anand Sinha, Yezi Liu, Ruijie Du, Athina Markopoulou, and Yanning Shen. Gradient inversion attack on graph neural networks. *Transactions on Machine Learning Research*, 2025.

[35] Yifan Sun and Meng Song. Differentially private graph convolutional networks with privacy amplification. In *2024 IEEE 23rd International Conference on Trust, Security and Privacy in Computing and Communications (TrustCom)*, pages 2327–2335, 2024.

[36] Leonid Nisonovich Vaserstein. Markov processes over denumerable products of spaces, describing large systems of automata. *Problemy Peredachi Informatsii*, 5(3):64–72, 1969.

[37] Thijs Vogels, Sai Praneeth Karimireddy, and Martin Jaggi. *PowerSGD: practical low-rank gradient compression for distributed optimization*. Curran Associates Inc., Red Hook, NY, USA, 2019.

[38] Cheng-Long Wang, Mengdi Huai, and Di Wang. Inductive graph unlearning. In *Proceedings of the 32nd USENIX Conference on Security Symposium, SEC '23, USA*, 2023. USENIX Association.

[39] Fan Wu, Yunhui Long, Ce Zhang, and Bo Li. Linkteller: Recovering private edges from graph neural networks via influence analysis. In *2022 IEEE Symposium on Security and Privacy (SP)*, pages 2005–2024, 2022.

[40] Felix Wu, Amauri Souza, Tianyi Zhang, Christopher Fifty, Tao Yu, and Kilian Weinberger. Simplifying graph convolutional networks. In *Proceedings of the 36th International Conference on Machine Learning*, pages 6861–6871. PMLR, 2019.

[41] Jiancan Wu, Yi Yang, Yuchun Qian, Yongduo Sui, Xiang Wang, and Xiangnan He. Gif: A general graph unlearning strategy via influence function. In *Proceedings of the ACM Web Conference 2023, WWW '23*, page 651–661, New York, NY, USA, 2023. Association for Computing Machinery.

[42] Zihang Xiang, Tianhao Wang, and Di Wang. Preserving node-level privacy in graph neural networks. In *2024 IEEE Symposium on Security and Privacy (SP)*, pages 4714–4732, 2024.

[43] Zhe-Rui Yang, Jindong Han, Chang-Dong Wang, and Hao Liu. Erase then rectify: a training-free parameter editing approach for cost-effective graph unlearning. In *Proceedings of the Thirty-Ninth AAAI Conference on Artificial Intelligence and Thirty-Seventh Conference on Innovative Applications of Artificial Intelligence and Fifteenth Symposium on Educational Advances in Artificial Intelligence, AAAI'25/IAAI'25/EAAI'25*. AAAI Press, 2025.

[44] Zhilin Yang, William Cohen, and Ruslan Salakhudinov. Revisiting semi-supervised learning with graph embeddings. In Maria Florina Balcan and Kilian Q. Weinberger, editors, *Proceedings of The 33rd International Conference on Machine Learning*, volume 48 of *Proceedings of Machine Learning Research*, pages 40–48, New York, New York, USA, 20–22 Jun 2016. PMLR.

[45] Hanyang Yuan, Jiarong Xu, Renhong Huang, Mingli Song, Chunping Wang, and Yang Yang. Can graph neural networks expose training data properties? an efficient risk assessment approach. In A. Globerson, L. Mackey, D. Belgrave, A. Fan, U. Paquet, J. Tomczak, and C. Zhang, editors, *Advances in Neural Information Processing Systems*, volume 37, pages 69361–69385. Curran Associates, Inc., 2024.

[46] Jiahao Zhang, Yilong Wang, Zhiwei Zhang, Xiaorui Liu, and Suhang Wang. Unlearning inversion attacks for graph neural networks, 2025.

[47] Qiuchen Zhang, Hong kyu Lee, Jing Ma, Jian Lou, Carl Yang, and Li Xiong. Dpar: Decoupled graph neural networks with node-level differential privacy. In *Proceedings of the ACM Web Conference 2024, WWW '24*, page 1170–1181, New York, NY, USA, 2024. Association for Computing Machinery.

[48] Rui Zhang, Song Guo, Junxiao Wang, Xin Xie, and Dacheng Tao. A survey on gradient inversion: Attacks, defenses and future directions. In Lud De Raedt, editor, *Proceedings of the Thirty-First International Joint Conference on Artificial Intelligence, IJCAI-22*, pages 5678–5685. International Joint Conferences on Artificial Intelligence Organization, 7 2022. Survey Track.

[49] Yuxing Zhang, Siyuan Meng, Chunchun Chen, Mengyao Peng, Hongyan Gu, and Xinli Huang. Link-thief: Combining generalized structure knowledge with node similarity for link stealing attack against gnn. In *Proceedings of the 32nd ACM International Conference on Multimedia, MM '24*, page 4947–4956, New York, NY, USA, 2024. Association for Computing Machinery.

[50] Zaixi Zhang, Qi Liu, Zhenya Huang, Hao Wang, Chee-Kong Lee, and Enhong Chen. Model inversion attacks against graph neural networks. *IEEE Transactions on Knowledge and Data Engineering*, 35(9):8729–8741, 2023.

[51] Zaixi Zhang, Qi Liu, Zhenya Huang, Hao Wang, Chengqiang Lu, Chuanren Liu, and Enhong Chen. Graphmi: Extracting private graph data from graph neural networks. In Zhi-Hua Zhou, editor, *Proceedings of the Thirtieth International Joint Conference on Artificial Intelligence, IJCAI-21*, pages 3749–3755. International Joint Conferences on Artificial Intelligence Organization, 8 2021. Main Track.

- [52] Zhikun Zhang, Min Chen, Michael Backes, Yun Shen, and Yang Zhang. Inference attacks against graph neural networks. In 31st USENIX Security Symposium (USENIX Security 22), pages 4543–4560, Boston, MA, August 2022. USENIX Association.
- [53] Ligeng Zhu, Zhijian Liu, and Song Han. Deep leakage from gradients. Curran Associates Inc., Red Hook, NY, USA, 2019.
- [54] Yuanxin Zhuang, Chuan Shi, Mengmei Zhang, Jinghui Chen, Lingjuan Lyu, Pan Zhou, and Lichao Sun. Unveiling the secrets without data: Can graph neural networks be exploited through Data-Free model extraction attacks? In 33rd USENIX Security Symposium (USENIX Security 24), pages 5251–5268, Philadelphia, PA, August 2024. USENIX Association.